Science Advances
AAAS

Supplementary Materials for

Childhood cancer mutagenesis caused by transposase-derived PGBD5

Makiko Yamada *et al.*

Corresponding author: Alex Kentsis, kentsisresearchgroup@gmail.com

Sci. Adv. **10**, eadn4649 (2024)
DOI: 10.1126/sciadv.adn4649

The PDF file includes:

Other Supplementary Material for this manuscript includes the following:

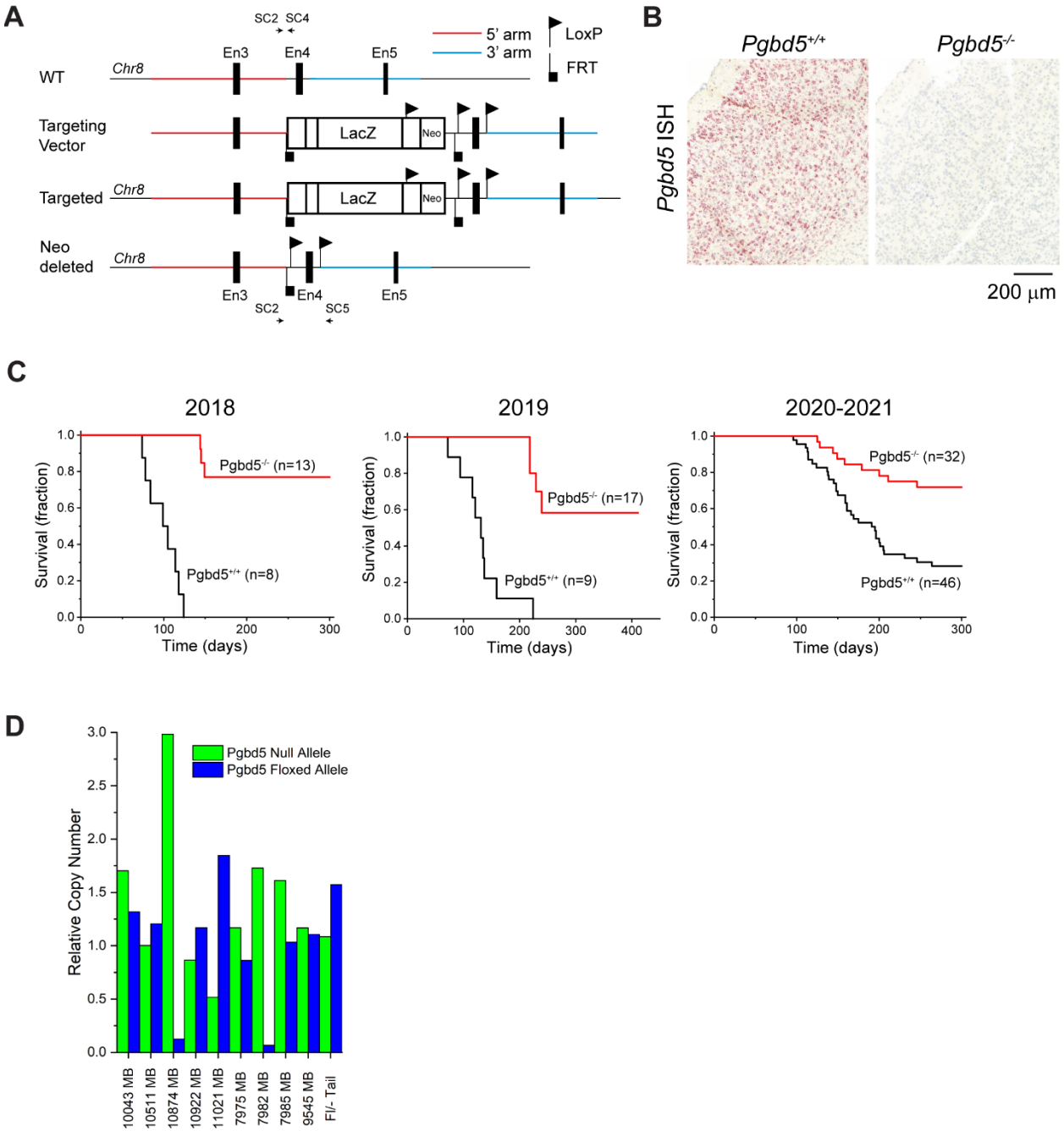

Fig. S1. Generation of *Pgbd5*$^{-/-}$ mice and the survival curves for the medulloblastoma model. (**A**) Generation of *Pgbd5*$^{-/-}$ mice. The top shows the *Pgbd5* wildtype (WT) gene locus including exon (En) 3-5 at chromosome 8. The targeted vector (second from top) consists of LacZ and neoR cassettes flanked by FRT sequences (black inverted square flag) and exon 4 flanked by LoxP sequences (black inverted triangle flag). Red and blue regions are 5' and 3' homology arms, respectively. The third line shows a successfully targeted gene locus which is confirmed by genotyping using SC2 and SC4 primers. These successfully targeted ES cell clones were microinjected into Balb/c blastocysts and resulting chimeras were crossed with FLP deleter mice to remove the LacZ and neoR cassettes. The bottom line shows the Pgbd5 floxed allele after

removal of the LacZ/neoR cassettes. This individual was crossed with an EIIa-Cre mice to generate global *Pgbd5*$^{-/-}$ mice, as confirmed by genotyping with SC2 and SC5 primers. (**B**) Representative images of the ISH using a BaseScope probe set against exon 4 of *Pgbd5* transcripts. Sagittal sections of *Pgbd5*$^{+/+}$ (left) and *Pgbd5*$^{-/-}$ (right) cortices show *Pgbd5*$^{+/+}$-specific signal in red. Nuclei were counter-stained with Hematoxylin (blue). (**C**) Three independent survival analyses in the *Ptch1*-mutant model conducted in 2018, 2019, and 2020-2021. *Pgbd5*$^{-/-}$ (red) mice exhibited significant protection from tumor development in all three cohorts (log-rank p = 3.0e-7, 1.0e-7, and 1.9e-4). The aggregated survival is shown in Fig. 1D. (**D**) Allele copy number analysis of nine *Pgbd5*$^{fl/-}$ tumor and one tail tissues by genomic qPCR. Green and blue indicates allele copy numbers of null and floxed alleles relative to those of *jun*, respectively. 10874 and 7982 tumors lost the floxed alleles while the other seven tumors retain the floxed alleles.

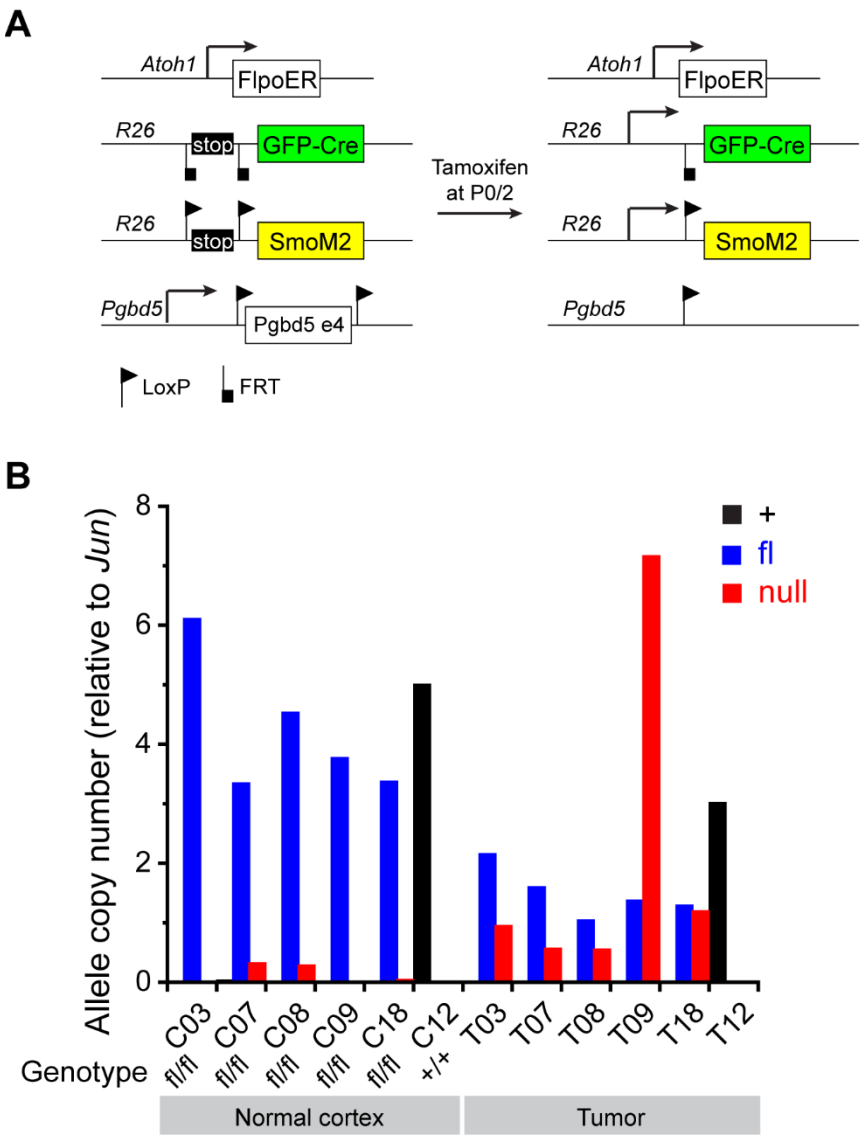

Fig. S2. The MASTR is the most stringent conditional approach to induce concurrent expression of *SmoM2* and deletion of *Pgbd5*. (**A**) Schematic showing strategy of the MASTR approach. Upon Tamoxifen injection at P0, FlpoER removes a stop cassette to drive GFP-Cre (green) expression, which induces SmoM2 protein (yellow) expression and concurrent deletion of *Pgbd5*. Triangle and square flags indicate LoxP and FRT sequences, respectively. (**B**) Allele copy number analysis of five normal cortices (left) and their corresponding tumors (right) by genomic qPCR. C03, C07, C08, C09, and C18 are $Pgbd5^{fl/fl}$; C12 is $Pgbd5^{+/+}$. Black, blue, and red indicate wildtype, floxed, and null alleles, respectively. In the tumors (T), except for T09, the floxed alleles are retained.

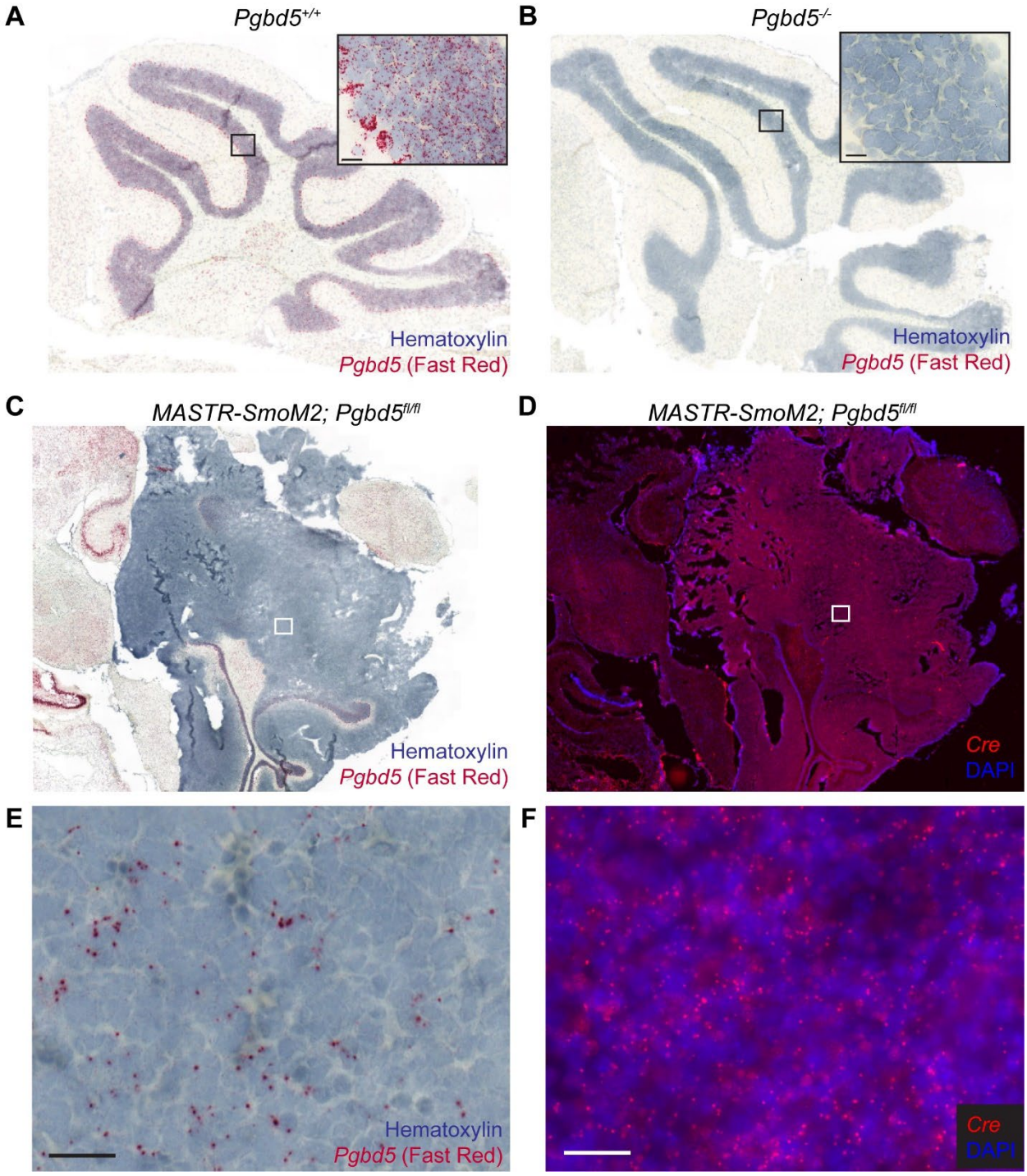

Fig. S3. Residual *Pgbd5* is observed in the MASTR tumor. (A&B) *In situ* hybridization (ISH) images of BaseScope *Pgbd5* probe set for *Pgbd5*$^{+/+}$ (positive control) (A) and *Pgbd5*$^{-/-}$ (negative control) (B) cerebella. *Pgbd5* signal is detected by Fast Red in *Pgbd5*$^{+/+}$ cerebellum whereas no signal is observed in *Pgbd5*$^{-/-}$. Nuclei are counterstained with hematoxylin. High magnification images are shown in the black insets. **(C)** Representative *Pgbd5* ISH image of a tumor from the *MASTR-SmoM2; Pgbd5*$^{fl/fl}$ mouse. **(D)** *Cre* FISH image of the adjoining section of (C). Red

fluorescence represents the *Cre* signal. Nuclei are counterstained with DAPI. **(E&F)** Higher magnification images of tumor areas (white rectangles) in (C) and (D), respectively. Residual *Pgbd5* signal is observed in the tumor (E) which is marked by the homogeneous *Cre* signal (F). Scale bars: 20 μm.

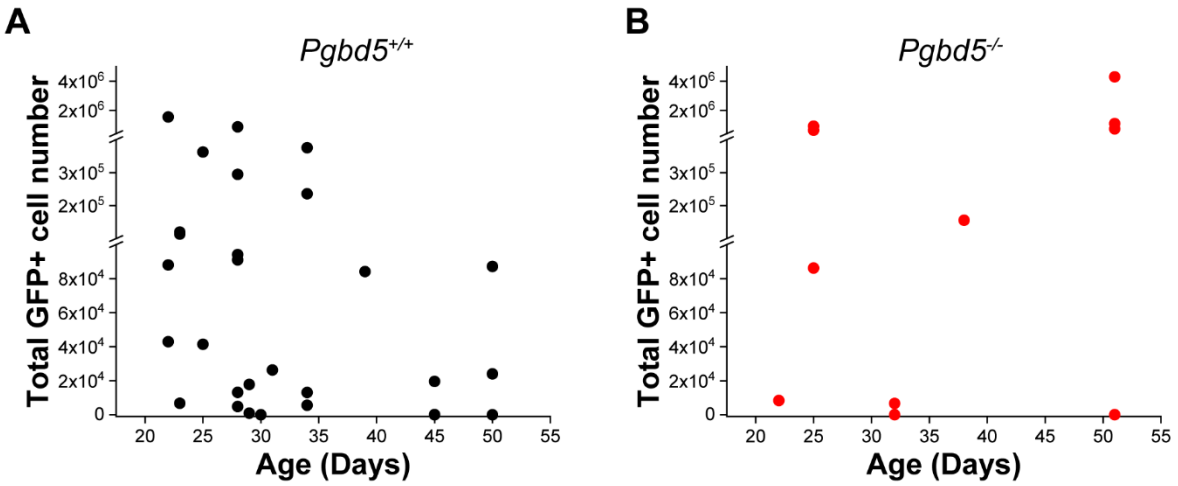

Fig. S4. Comparable Atoh1-GFP+ cell numbers in the *Pgbd5*$^{+/+}$ and *Pgbd5*$^{-/-}$ cerebella. Total Atoh1-GFP+ cell numbers in the *Pgbd5*$^{+/+}$ (**A**) and *Pgbd5*$^{-/-}$ (**B**) cerebella between 3 and 8 weeks by FACS. Both show similar numbers of the total Atoh1-GFP+ cells (t-test $p = 0.16$).

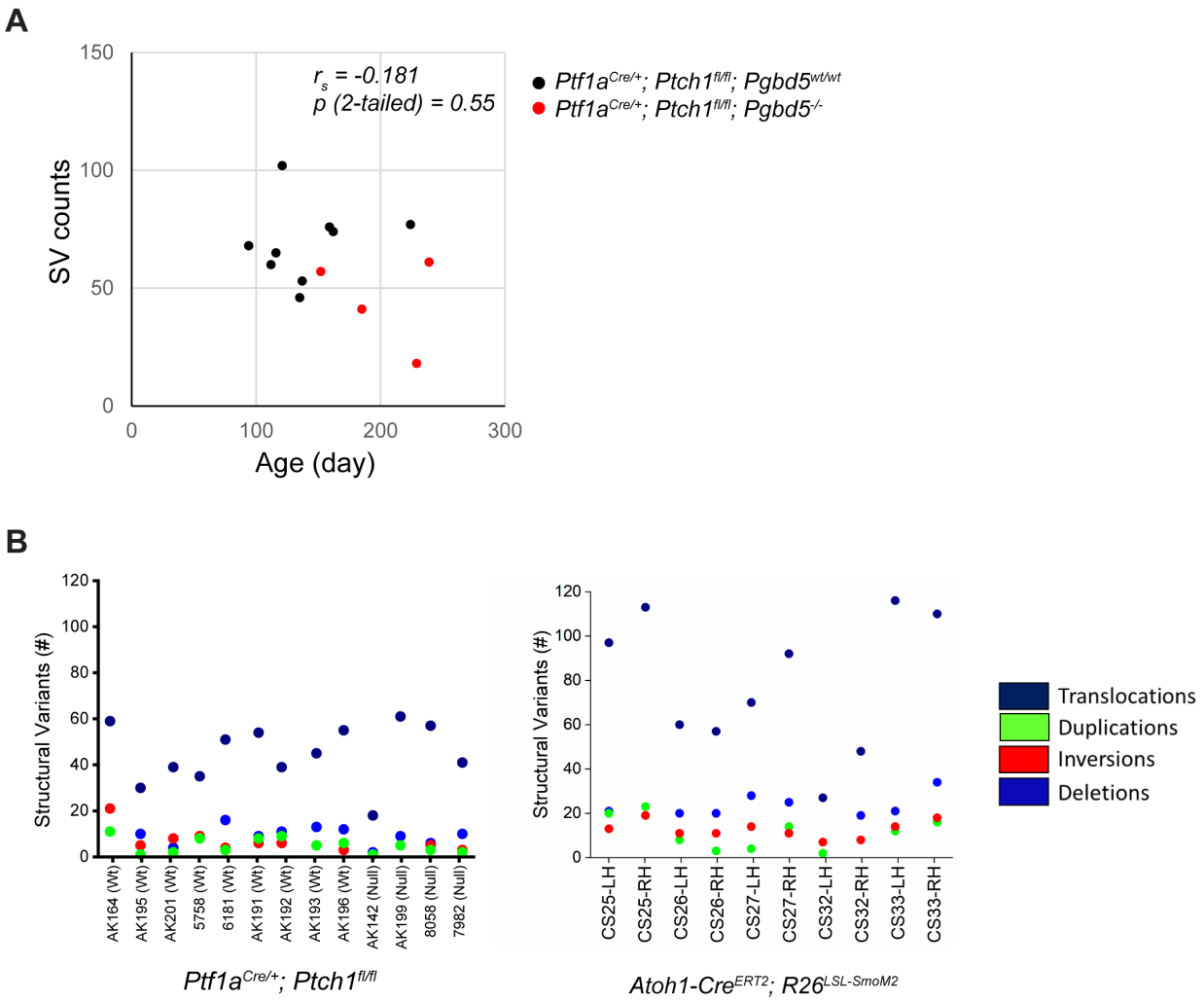

Fig. S5. No significant correlation between age and numbers of structural variants. (**A**) Scatter plot showing the relationship between the age of tumors and numbers of somatic structural variants in the *Ptch1*-mutant model. Both *Pgbd5*$^{+/+}$ (black) and *Pgbd5*$^{-/-}$ (red) tumors did not show significant correlation between age and numbers of structural variants. (**B**) Numbers of different types of structural variants in *Ptch1*- (left) and *SmoM2*-mutant (right) tumors. Both models show similar numbers of mutation types regardless of the presence of Pgbd5.

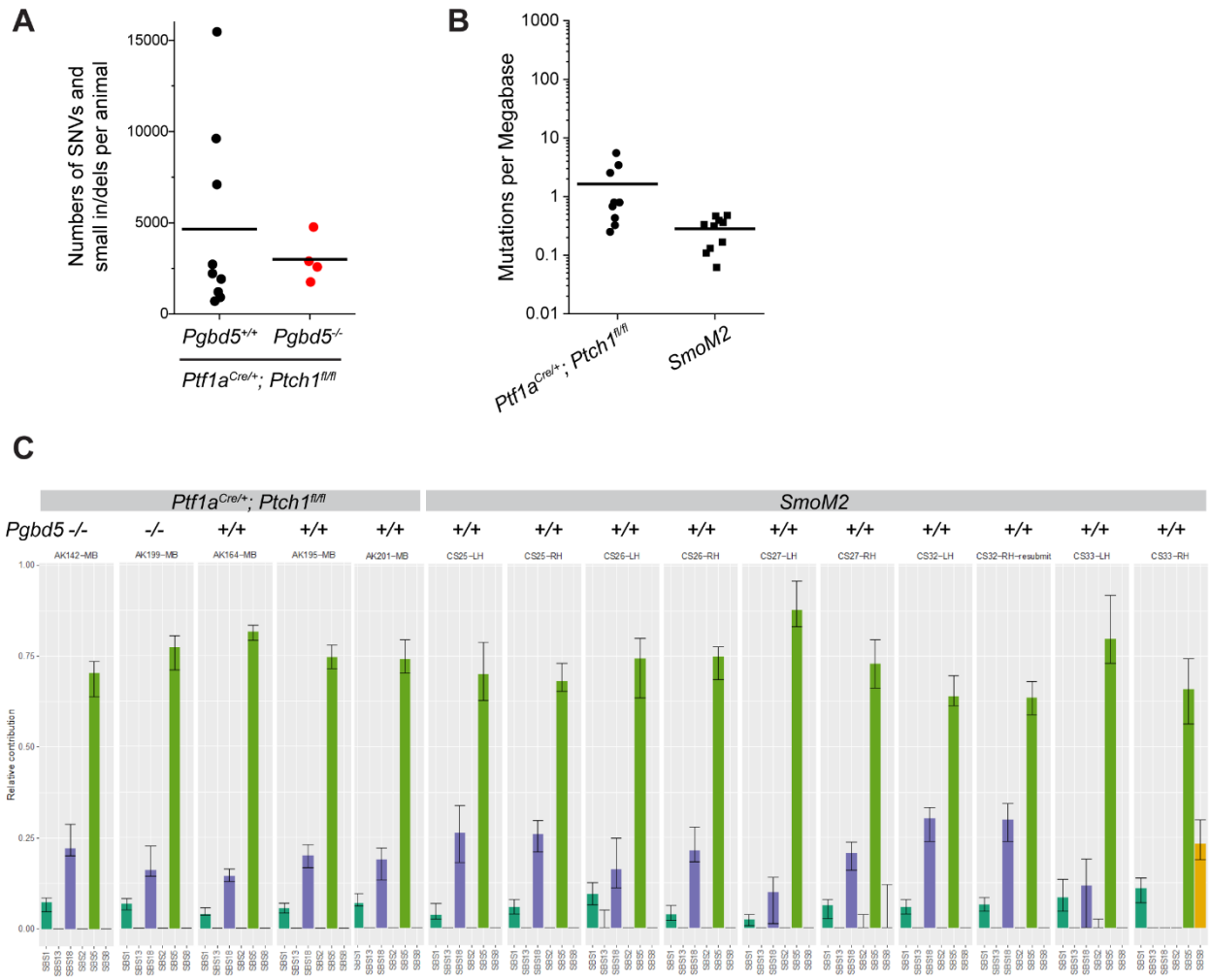

Fig. S6. Analyses of numbers of SNVs and mutational signatures. (A) Comparison of numbers of SNVs and small indels between *Pgbd5*$^{+/+}$ (black: N = 9) and *Pgbd5*$^{-/-}$ (red: N = 4) *Ptch1*-mutant tumors. Both tumors have similar numbers of SNVs and small indels. Bars indicate means. **(B)** Comparison of numbers of SNVs and small indels between *Ptch1*- (N = 9) and *SmoM2*- (N = 10) mutant tumors. Both tumors show relatively low numbers of mutations. **(C)** Mutational signature analysis. Ratios of contribution of the major signatures found in SNVs. The left five are from the *Ptch1*-mutant tumors (2 *Pgbd5*$^{-/-}$ and 3 *Pgbd5*$^{+/+}$) and the right ten are from the *SmoM2*-mutant tumors. SBS1; dark green, SBS5; light green, SBS18; purple, SBS8; orange. SBS5 is the most dominant signature, followed by SBS18 and SBS1. The only exception is *SmoM2*-mutant CS33-RH exhibiting the SBS8 contribution instead of SBS18.

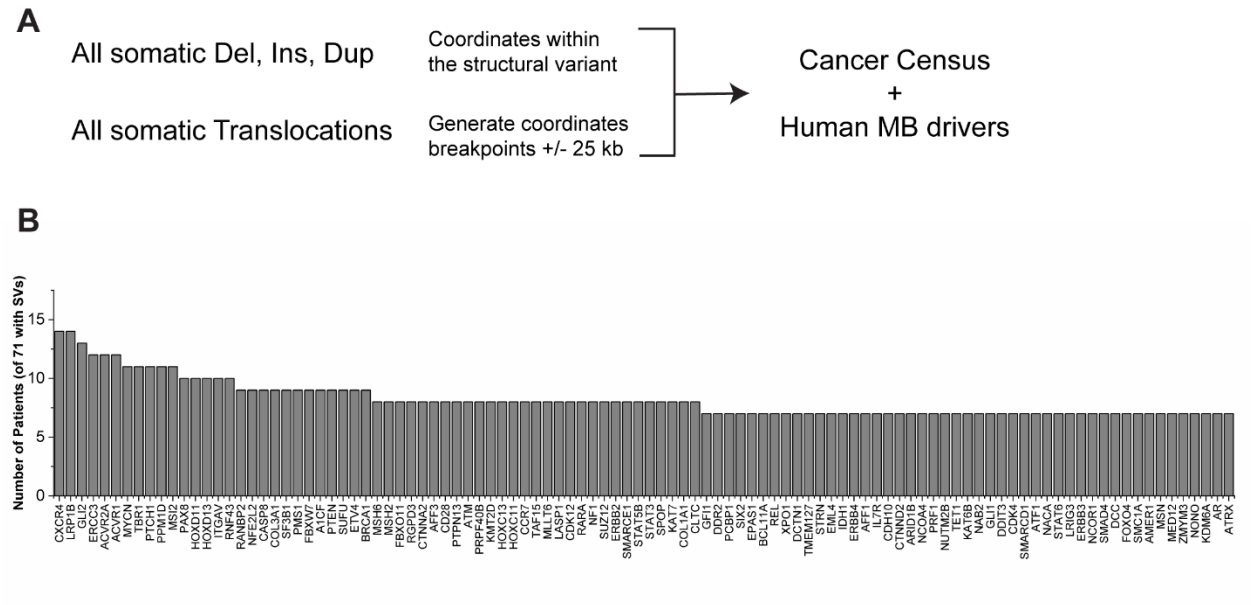

Fig. S7. Cancer census genes affected by somatic structural variants in a cohort of human SHH medulloblastomas. (**A**) Schematic to identify genes putatively affected by SVs. Genes were considered affected by structural variants if the gene was intersected by a structural variant breakpoint, if the gene was between a duplication, inversion, or deletion, or if the gene was within 25kb of a translocation breakpoint. (**B**) Many recurrent medulloblastoma tumor suppressors and oncogenes are affected by SVs. In the cohort of SHH subtype medulloblastoma (Fig. 4A), 71 tumors had structural variants. Genes known to be recurrently affected in human medulloblastomas are affected in >10% of cases, including *CXCR4, MYCN, PPM1D, PTCH1, GLI2*, and others.

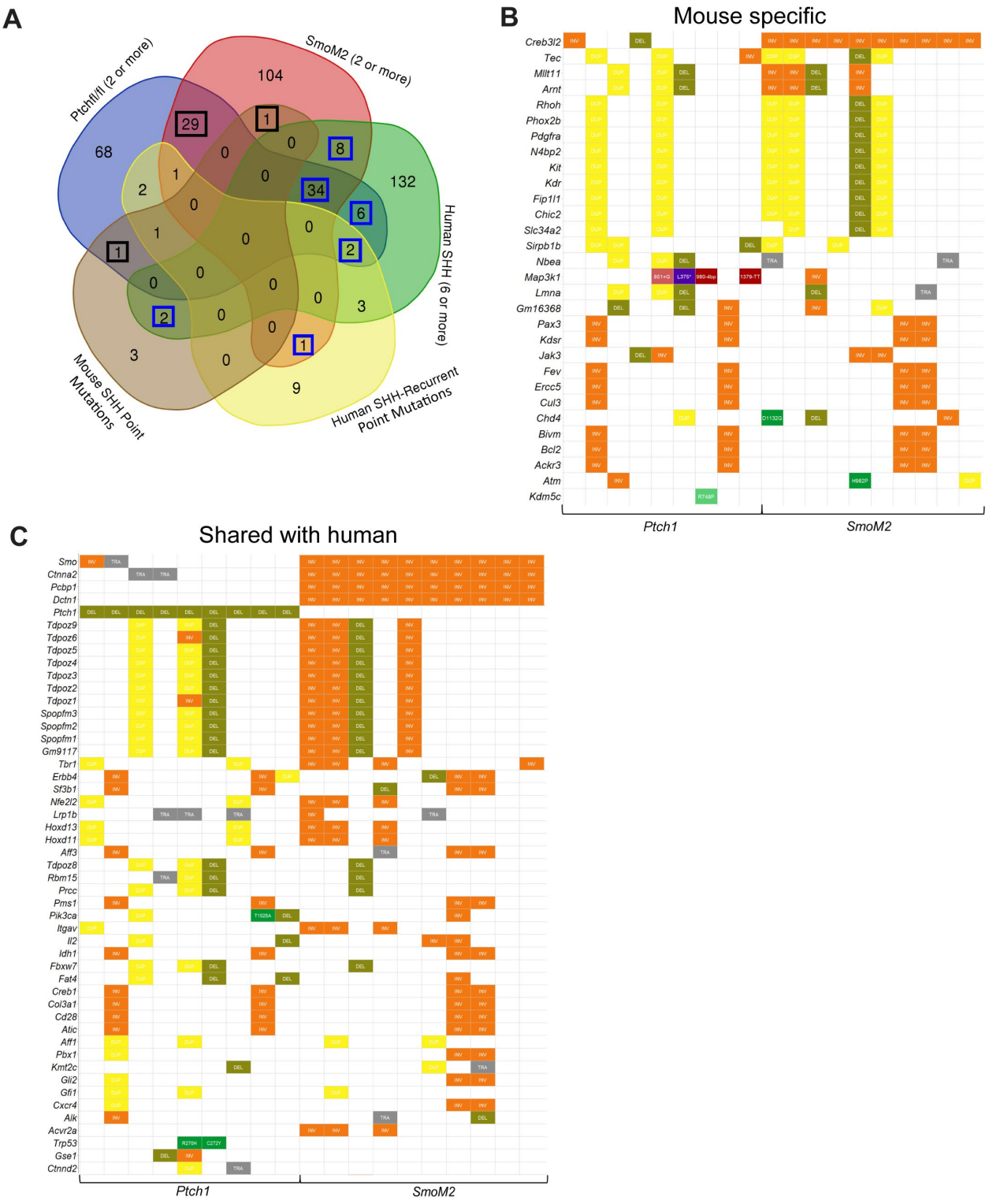

Fig. S8. Genes recurrently affected by somatic structural variants in human medulloblastoma are also affected in *Pgbd5*$^{+/+}$; *Ptch*$^{fl/fl}$ medulloblastomas and *SmoM2*-mutant medulloblastoma. (**A**) Venn diagram depicting the overlap among cancer census genes between human medulloblastomas and each mouse tumor model, including those affected by structural variants and point mutations. The numbers boxed in black are mouse specific genes (B),

and the numbers boxed in blue represent overlaps between human and mouse tumors (C). (**B**) Genes affected in two or more mouse tumors that are not affected by structural variants in more than 10% of SHH medulloblastomas in this cohort. Affected genes are chosen with the same criteria as in Fig. S7A. (**C**) Set of genes affected in both human and mouse medulloblastomas, including structural variants and point mutations.

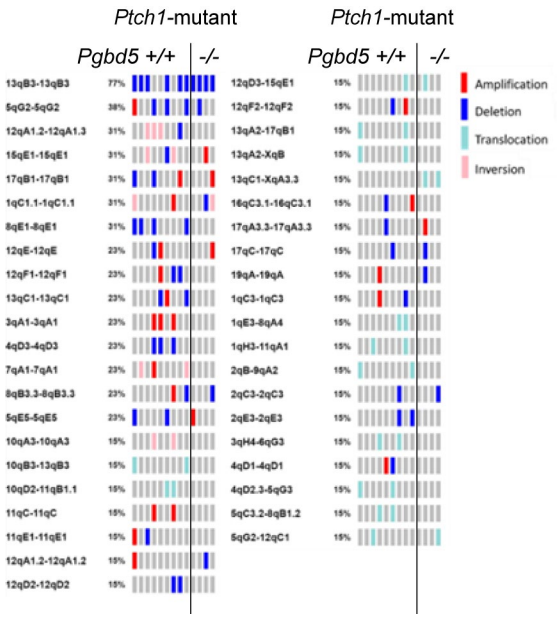

Fig. S9. Oncoprint depicting recurrently affected genomic regions (cytobands), stratified by structural variant type, in *Ptch1*-mutant tumors. The left nine and right four columns indicate tumors from *Pgbd5*$^{+/+}$ and *Pgbd5*$^{-/-}$ mice, respectively. Red, blue, light blue, pink, and gray symbols indicate amplifications, deletions, translocations, inversions, and no alteration, respectively.

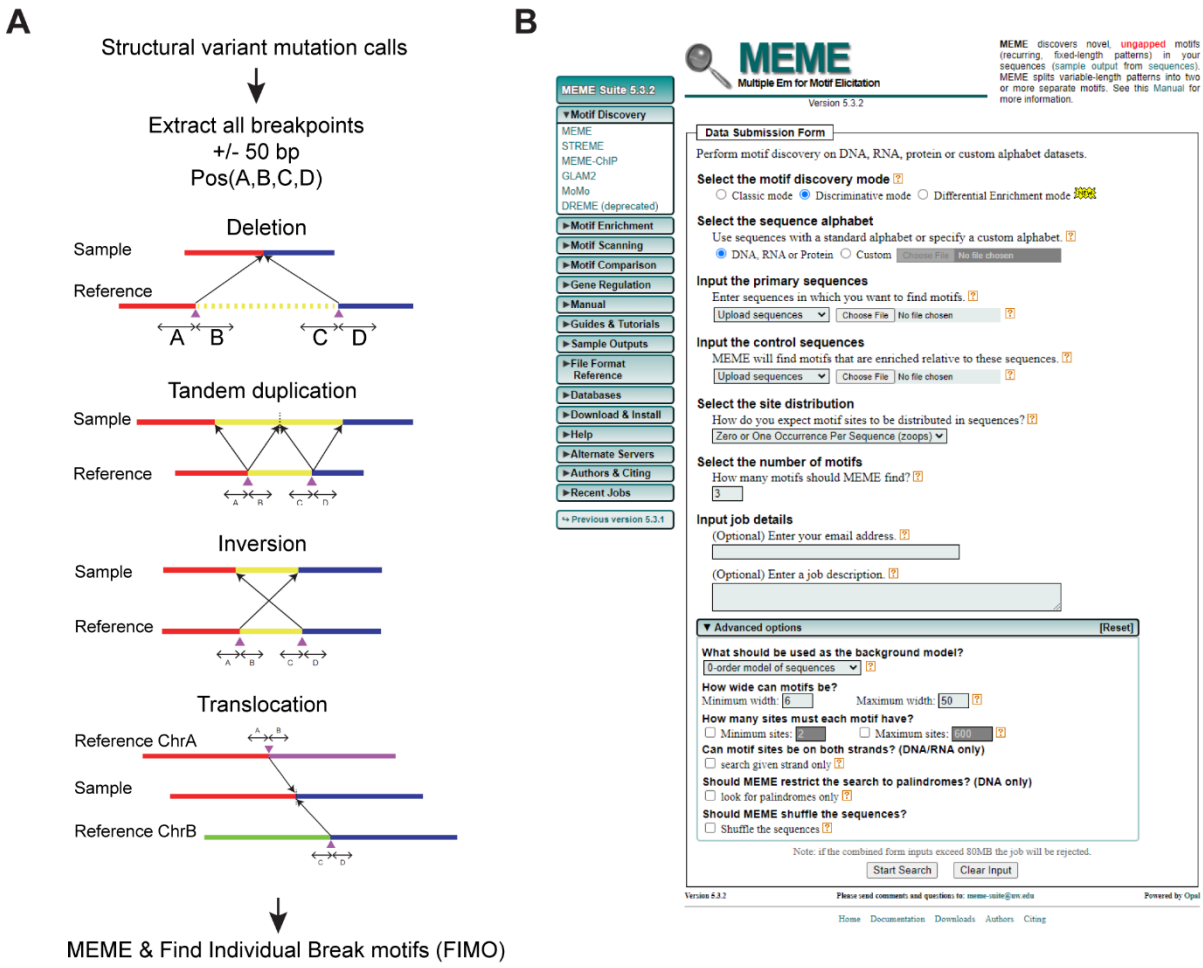

Fig. S10. Methods for breakpoints analyses. (A) Schematic describing the method used to extract 50mer flanking sequences from structural variant breakpoints in mouse medulloblastoma genomes. Following somatic mutation detection, 50mer sequences were extracted using bedtools in FASTA format compatible with MEME (see methods). **(B)** Depiction of paremters for MEME analysis. Discriminative MEME was used with default settings. *Pgbd5*-wildtype tumor 50mers were used as the primary sequences (2480 50mers) and *Pgbd5*$^{-/-}$ tumor 50mers were used as the control sequences (708 50mers). MEME was used with 11, 12, 13, 14, 15, and 16 maximum base pairs. Repetitive sequences were eliminated and specific sequences were chosen as putative *Pgbd5* specific motifs.

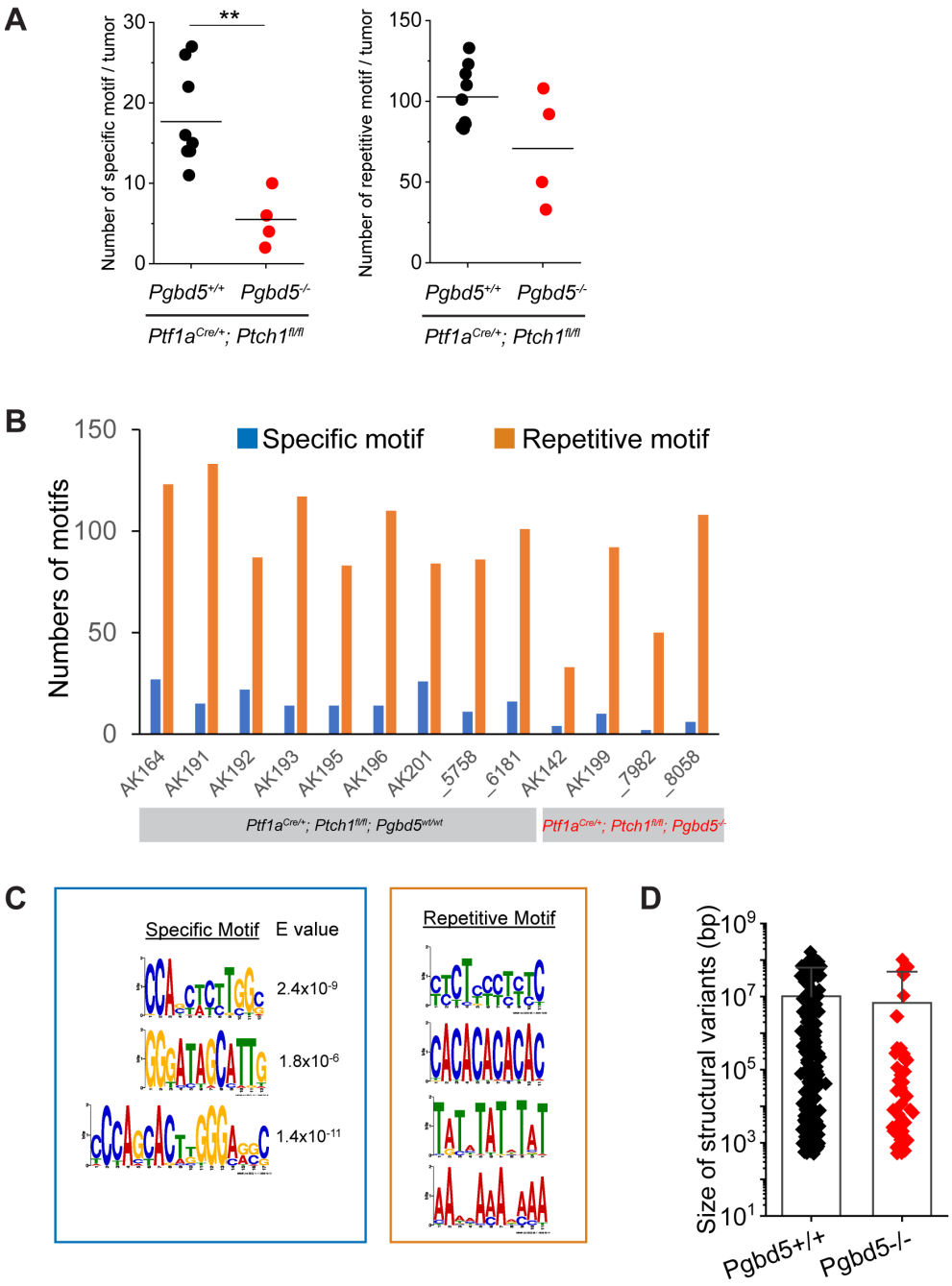

Fig. S11. Comparisons of numbers of the specific and repetitive motifs between *Pgbd5*$^{+/+}$ and *Pgbd5*$^{-/-}$ Ptch1-mutant tumors. (**A**) Comparison of the number of Pgbd5-specific motifs shown in the left diagram of (C) between *Pgbd5*$^{+/+}$ (black) and *Pgbd5*$^{-/-}$ (red) *Ptch1*-mutant tumors (Left graph). *Pgbd5*$^{+/+}$ tumors harbor more specific motifs (t-test p = 2.7e-3). Right graph shows comparison of numbers of the repetitive motifs shown in the right diagram of (C) between *Pgbd5*$^{+/+}$ and *Pgbd5*$^{-/-}$ tumors. No significant difference in the number of repetitive motifs was observed. (**B**) Numbers of motifs in each tumor from the *Ptch1*-mutant model. Left nine and right four tumors are from *Pgbd5*$^{+/+}$ and *Pgbd5*$^{-/-}$ mice, respectively. Blue indicates the total numbers of the three Pgbd5-specific motifs depicted in the left of (C) and orange indicates total numbers of

the repetitive motifs shown in the right diagram of (C). **(D)** Size of structural variants in the *Ptch1*-mutant model. Error bars indicate standard deviations.

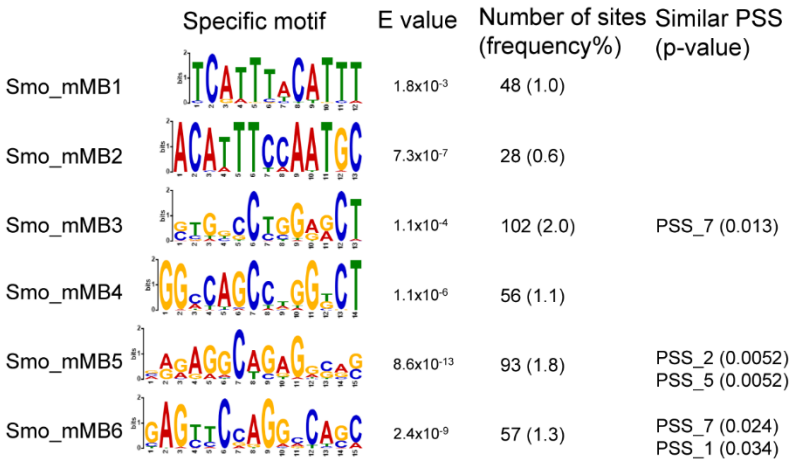

Fig. S12. Specific motifs identified in *SmoM2*-mutant tumors share similarity with previously identified PSS motifs. E-value indicates significance based on the number of motifs that are expected should the motifs be shuffled. Frequency is the instance number within the set of breakpoint 50mers. Some of these motifs were similar to previously identified PSS motifs, as measured using TomTom .

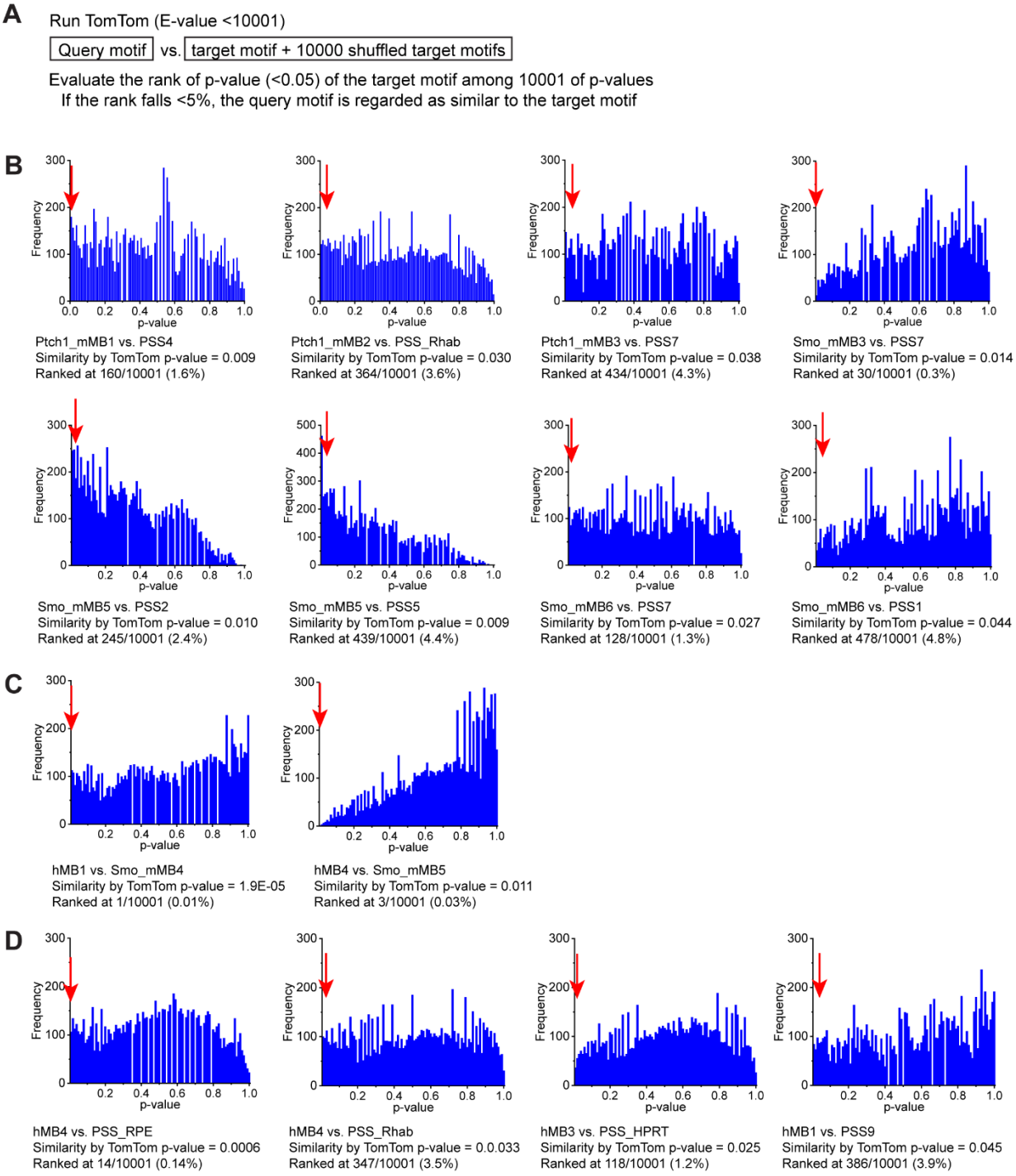

Fig. S13. Verification of similarities among breakpoint motifs. (**A**) Method description on how the similarity is verified. The shuffled target motifs were used as background. If the *p*-value of a target motif falls within the lowest 5% of all p-values, the similarity is verified. (**B**) Histograms of all the *p*-values (target motif plus its 10,000 shuffled motifs) for mouse medulloblastoma (mMB) motifs vs. previously identified PSS motifs. Red arrows point to the *p*-value of target motifs. The *p*-value and its ranking are shown under the histogram. (**C**) Comparison of human medulloblastoma (hMB) motifs vs. mMB motifs. (**D**) Comparisons of hMB motifs vs. previously identified PSS motifs.

A

MEME Suite 5.0.5

FIMO

Find Individual Motif Occurences

Version 5.0.5

FIMO scans a set of sequences for individual matches to each of the motifs you provide (sample output for motifs and sequences). See this Manual or this Tutorial for more information.

Motif ID	Alt ID	Sequence	Strand	Start	End	p-value	q-value	Matched Sequence
1	GWAATCC	AK164_48	-	3	13	2.05E-07	0.00541	GTAATCCCAGC
1	GWAATCC	AK164_48	-	3	13	2.05E-07	0.00541	GTAATCCCAGC
1	GWAATCC	AK164_59	-	34	44	3.39E-06	0.0597	ATAACCCCAGC
1	GWAATCC	AK164_18	+	30	40	0.0000159	0.21	caaatcccagc
1	GWAATCC	AK164_71	-	12	22	0.0000395	0.401	GCAAGCCCAGC
1	GWAATCC	AK164_33	+	5	15	0.0000455	0.401	ttgatcccagc
1	GWAATCC	AK164_16	-	4	14	0.0000745	0.5	GTAACGCCATC
1	GWAATCC	AK164_82	-	10	20	0.0000757	0.5	GAACTCCCATC
1	GWAATCC	AK164_26	-	19	29	0.0000852	0.5	GCATCCCCAGC

B

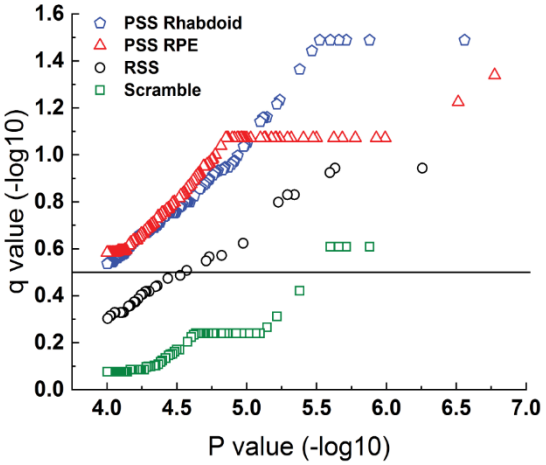

C

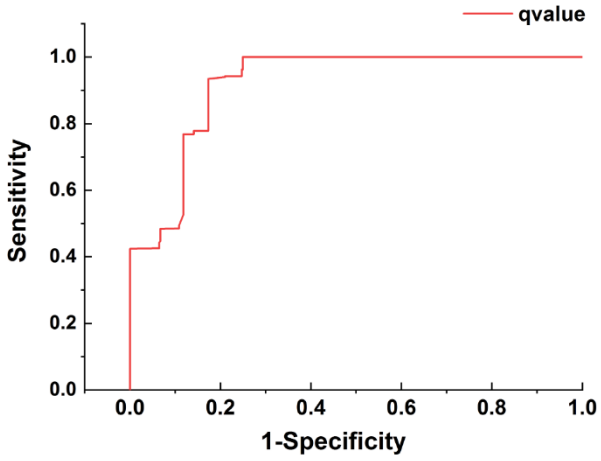

Fig. S14. FIMO analysis and its validation method. (**A**) An example of FIMO analysis. The *q*-value is a modification of the *p*-value, corrected for the respective false discovery rate. Each row represents a sequence that matched to the queried motif. (**B**) Graphical representation of the output when 50mers from human SHH subtype structural variants were queried with different motifs, including previously identified PSS motifs (Rhabdoid and RPE) and motifs known not to be associated with Pgbd5 activity, including the RAG1/2 specific signal sequence and a scrambled motif. The line indicates the *q*-value above which all sequences with PSS sequences are correctly identified, with negligible number of negative control sequences. This threshold was chosen as the q-value for breakpoint sequence motif identification. (**C**) Receiver operating characteristic curve analysis of values from (B), demonstrating the separation of PSS sequences from negative controls with 100% sensitivity and 75% specificity using q-value cutoff of 0.3.

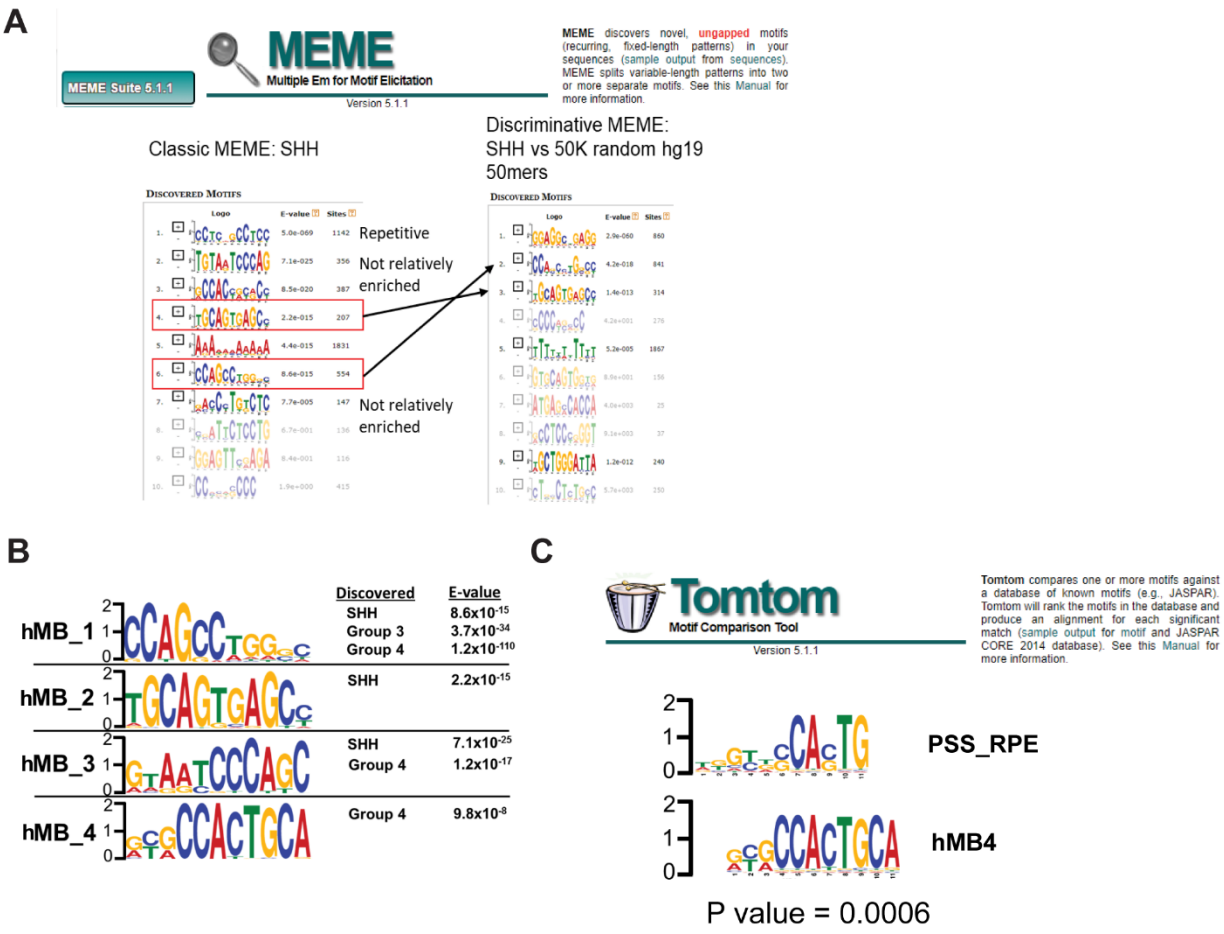

Fig. S15. Specific sequence motifs enriched in human medulloblastomas at structural variant breakpoints. (**A**) Example output from MEME and method for eliminating repetitive motifs. Motifs were chosen based on whether they were sequence-specific (i.e., not repetitive) and whether they were enriched using discriminative MEME relative to a set of 50,000 50mers randomly sampled from the hg19 reference genome. (**B**) Specific motifs identified in human medulloblastomas. The "discovered" column describes the subtype of medulloblastoma where the motif was initially discovered based on the method in A. The *E*-values list strengths of apparent associations. (**C**) Example of motif comparison between a de novo discovered motif (hMB_4) and a previously identified Pgbd5-specific signal sequence motif (PSS_RPE).

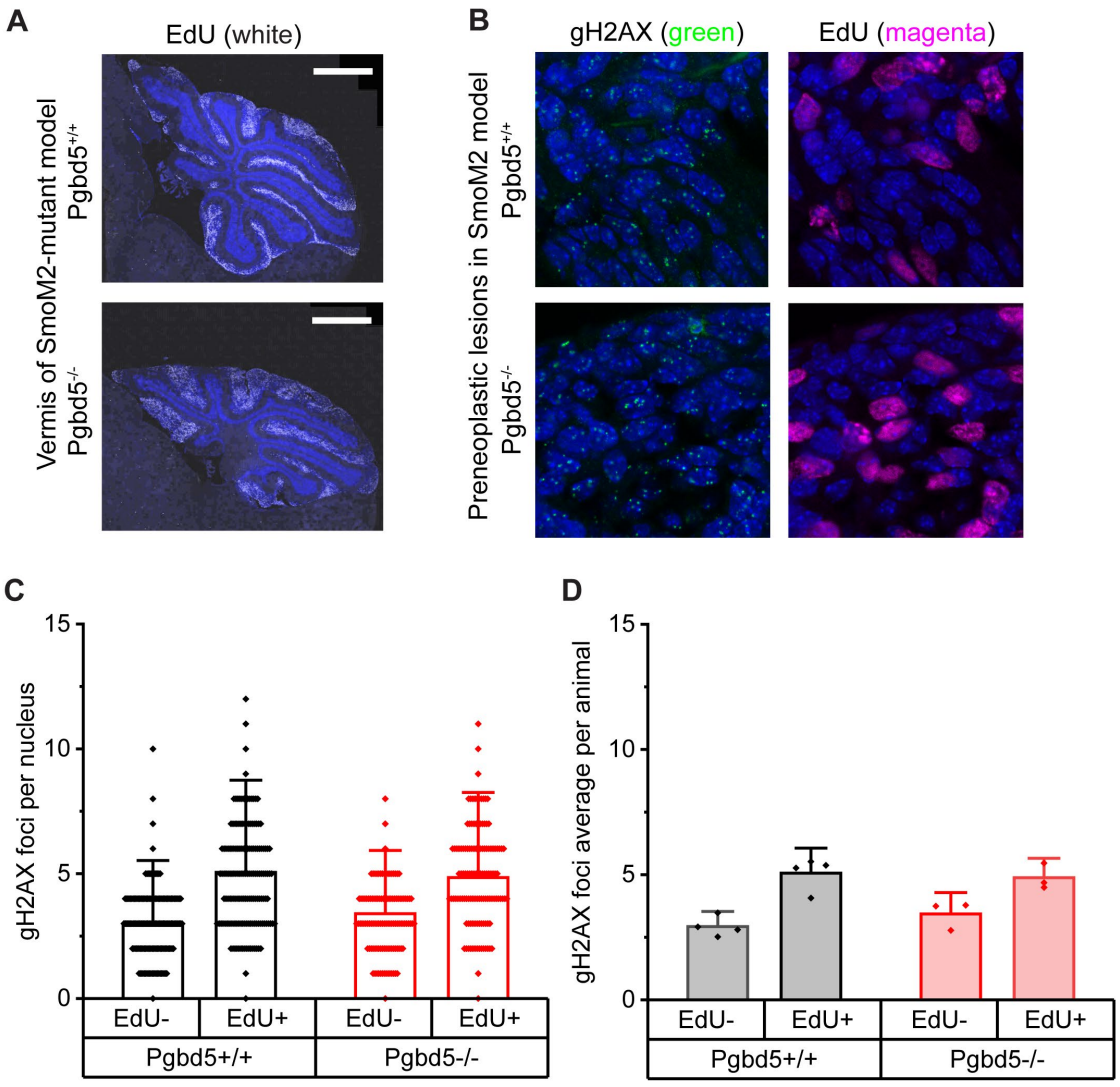

Fig. S16. Counting gH2AX foci in the preneoplastic GCPs from *SmoM2*-mutant model at P22/23. (A) Representative images of the vermis from *Atoh1-CreER^{T2}; R26SmoM2* mice. Preneoplastic lesions are morphologically distinguishable by the outermost cell layer that does not exist in normal cerebellum at P22/23. The preneoplastic lesions contain dividing cells which are stained by EdU (white). Scale bar: 1mm. **(B)** Representative images of gH2AX (green) and EdU (magenta) double staining of preneoplastic lesions. DAPI was used to stain DNA. Top two and bottom two panels are from a *Pgbd5$^{+/+}$* and *Pgbd5$^{-/-}$* mouse, respectively. Scale bar: 10 μm. **(C)** Graph showing gH2AX foci counts per nucleus for EdU-negative and positive nuclei from *Pgbd5$^{+/+}$* (black dots, n=360 nuclei from n=4 mice) and Pgbd5$^{-/-}$ (red dots, n=270 nuclei from n=3 mice) preneoplastic cells. EdU-negative *Pgbd5$^{+/+}$* vs. *Pgbd5$^{-/-}$*; t-test p=0.02; EdU-positive *Pgbd5$^{+/+}$* vs. *Pgbd5$^{-/-}$*; t-test p=0.44. **(D)** Graph showing average gH2AX foci counts per animal. Both *Pgbd5$^{+/+}$* (n=4) and *Pgbd5$^{-/-}$* (n=3) animals show similar counts in gH2AX foci. EdU-negative *Pgbd5$^{+/+}$* vs. *Pgbd5$^{-/-}$*; t-test p=0.22; EdU-positive *Pgbd5$^{+/+}$* vs. *Pgbd5$^{-/-}$*; t-test p=0.72. Error bars represent standard deviations.

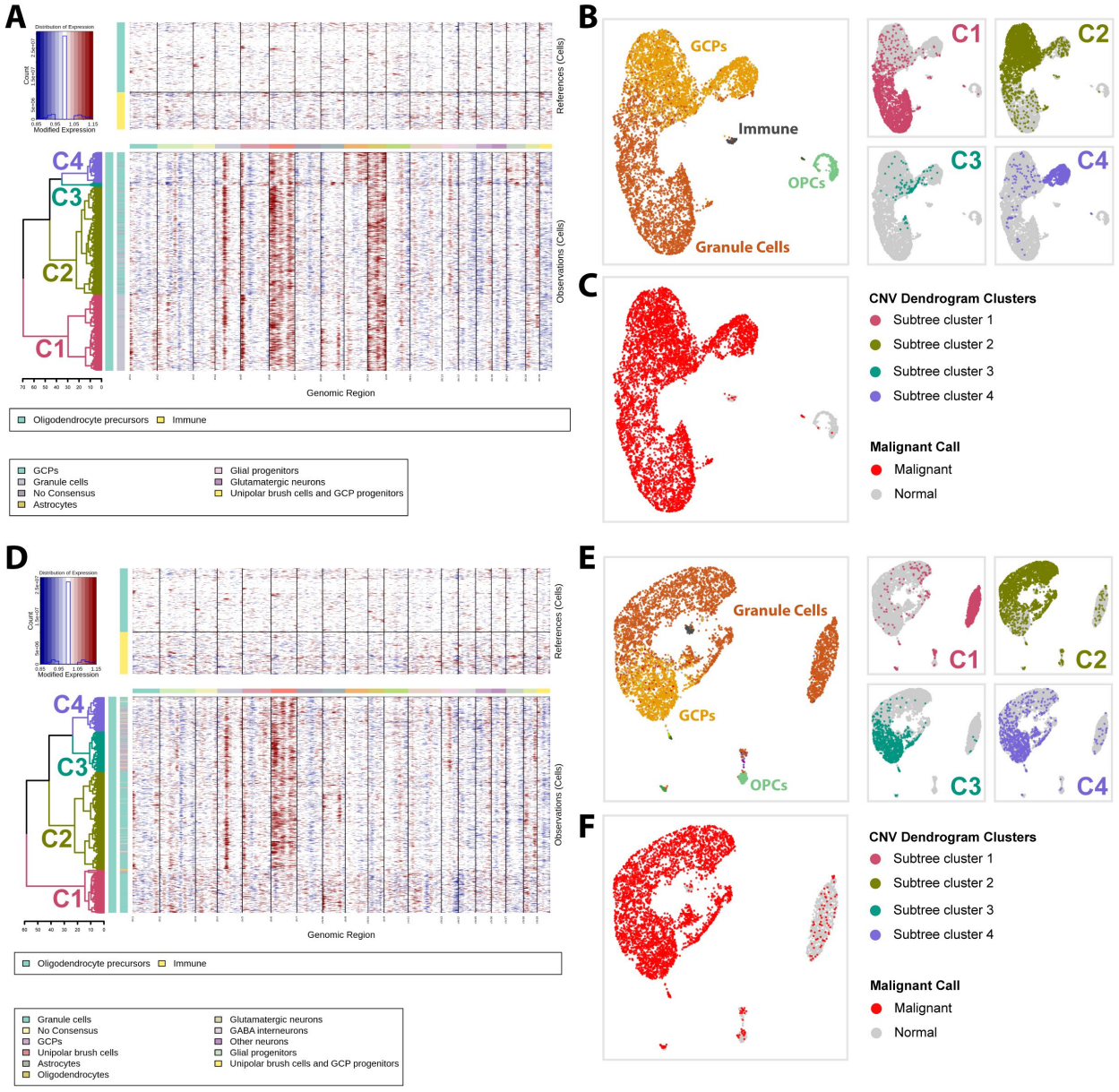

Fig. S17. Identification of malignant cells through inferred copy number variants (CNV). CNVs were called within each singe cell multiome sample using inferCNV tool and their corresponding single nuclei RNA-seq data. Malignant cell identification is shown for a sample (MY-2015-7982) where all inferred cells were malignant (A-C). **(A)** Heatmap generated by inferCNV tool with denoising method applied. Chromosomal amplifications are inferred from red blocks of expression, while deletions are inferred from blue blocks. Top: baseline expression values across chromosomal regions for the normal reference cells. Bottom: expression of non-reference cells. Left: Dendrogram for the non-reference cells cut into subtree clusters (k = 3). (B,C) UMAP plots of corresponding sample (N = 6,786). **(B)** Left: Cells are colored by cell class annotations. Right: Cells are colored by their corresponding subtree cluster from inferCNV heatmap. **(C)** Cells are colored by malignant calls based on the presence of CNV alterations observed. Malignant cell identification as in (A-C) in a different sample (MY-2015-8053) where

inferred cells clustered based on noticeable CNV alterations and by lack of alterations, corresponding to malignant and normal cells, respectively (D-F).

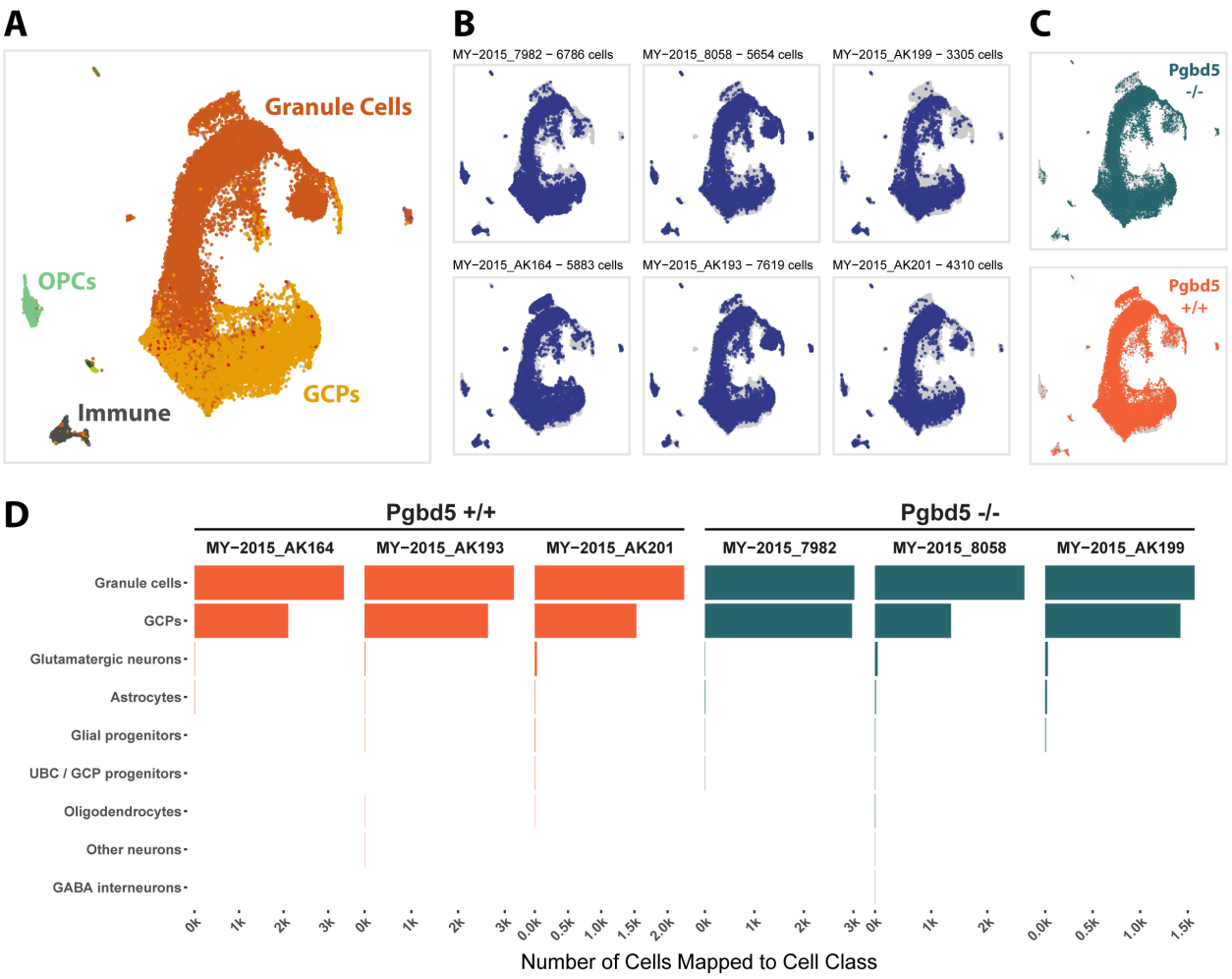

Fig. S18. *Pgbd5*$^{+/+}$ and *Pgbd5*$^{-/-}$ medulloblastomas belong to the granule cell lineage. (A-C) UMAP plots of single nuclei RNA-seq of *Pgbd5*$^{+/+}$ (N = 17,812) and *Pgbd5*$^{-/-}$ (N = 15,745) medulloblastomas samples. (A) Cells are colored by cell class annotations. (B) Cells pertaining to each sample are highlighted. (C) Malignant cells belonging to *Pgbd5*$^{+/+}$ (bottom) and *Pgbd5*$^{-/-}$ (top) genotype are highlighted. (D) Bar plots depicting the cell class consensus predictions for the malignant cells in each sample.

Table S1.
Combinations of similar motifs by motif comparison.

Motif ID	No. of sites (%frequency)	Similar PSS	p-value	p-value ranking among 10001 shuffled motifs (%rank)
Mouse motifs				
Ptch1_ mMB1	69 (2.8)	PSS_4	7.60E-03	160 (1.6)
Ptch1_mMB2	42 (1.7)	PSS_Rhab	4.54E-02	364 (3.6)
Ptch1_mMB3	38 (1.5)	PSS_7	2.42E-02	434 (4.3)
Smo_mMB3	102 (2.0)	PSS_7	1.32E-02	30 (0.3)
Smo_mMB5	93 (1.8)	PSS_2	5.20E-03	245 (2.4)
Smo_mMB5	93 (1.8)	PSS_5	5.20E-03	439 (4.4)
Smo_mMB6	57 (1.3)	PSS_7	2.36E-02	128 (1.3)
Smo_mMB6	57 (1.3)	PSS_1	3.39E-02	478 (4.8)
Human motifs				
hMB1	1957 (6.3)	Smo_mMB4	5.30E-06	1 (0.01)
hMB4	785 (2.5)	Smo_mMB5	1.04E-02	3 (0.03)
Human motifs				
hMB4	785 (2.5)	PSS_Rhab	3.32E-02	347 (3.5)
hMB4	785 (2.5)	PSS_RPE	6.03E-04	14 (0.14)
hMB1	1957 (6.3)	PSS_9	4.51E-02	386 (3.9)
hMB3	1274 (4.1)	PSS_HPRT	2.52E-02	118 (1.2)

Table S2.
Affected putative driver genes associated with Pgbd5-specific motifs.

Gene	References	Sample	SV type	SV location	Motif
Smo	Northcott et al (*78*), many others	AK192	TRA	chr6: 29749194-chr13:74529530	PSS_Rhab, PSS_RPE
		AK195	INV	chr6: 3136615-52335113	Ptch1_mMB2
Nrg1	Gilbertson et al (*79*), Aldaregia et al (*80*), Gu et al (*81*)	AK192	DEL	chr8: 27353926-37114336	Ptch1_mMB2
		AK196	INV	chr8: 28362263-37097181	PSS_Rhab, PSS_RPE
		AK164	DEL	chr8: 23477067-123425802	Ptch1_mMB2, PSS_Rhab, PSS_RPE
Wrn	Fukushima et al (*82*), Kloosterman et al (*83*)	AK192	DEL	chr8: 27353926-37114336	Ptch1_mMB2
		AK196	INV	chr8: 28362263-37097181	PSS_Rhab, PSS_RPE
		AK164	DEL	chr8: 23477067-123425802	Ptch1_mMB2, PSS_Rhab, PSS_RPE
Muc1 Ntrk1 Bcl9 Fbxw7 Tdpoz1-9 Arnt	Thomaz et al (*84*) for Ntrk1	5758	DUP	chr3: 61656127-98398034	Ptch1_mMB2
Lrp1b	Northcott et al (*85*)	AK201	TRA	chr2: 42665203-chr9:83248869	Ptch1_mMB2
Gfi1 Ptpn13 Aff1	Northcott et al (*86*)	AK164	DUP	chr5: 43061691-137976554	Ptch1_mMB1

Data S1. (separate file)
SNVs and indels from WGS of Ptch1-mutant mouse MBs
Data S2. (separate file)
SVs from WGS of Ptch1-mutant mouse MBs
Data S3. (separate file)
SNVs and indels from WGS of SmoM2-mutant mouse MBs
Data S4. (separate file)
SVs from WGS of SmoM2-mutant mouse MBs
Data S5. (separate file)
Cancer census genes affected by SVs in mouse MBs
Data S6. (separate file)
50mer sequences extracted from mouse WGS
Data S7. (separate file)
MEME results with the 50mer seqs of SVs from Ptch1-mutant Pgbd5+/+ and Pgbd5-/- mice
Data S8. (separate file)
Cancer census genes affected by SVs in human SHH-MBs
Data S9. (separate file)
50mer sequences of SVs from human SHH-MBs
Data S10. (separate file)
50mer sequences of SVs from human Group3-MBs
Data S11. (separate file)
50mer sequences of SVs from human Group4-MBs
Data S12. (separate file)
50mer sequences of SVs from human WNT-MBs
Data S13. (separate file)
50mer sequences of SVs from human breast carcinoma
Data S14. (separate file)
FIMO output from human SHH-MBs
Data S15. (separate file)
FIMO output from human Group3-MBs
Data S16. (separate file)
FIMO output from human Group4-MBs
Data S17. (separate file)
FIMO output from human WNT-MBs
Data S18. (separate file)
FIMO output from human breast carcinoma
Data S19. (separate file)
SV IDs and corresponding 50mers for select MB oncogenes and suppressors
Data S20. (separate file)
Cytoband analysis of SVs
Data S21. (separate file)
Single-cell multiome ATAC + gene expression analysis
Data S22. (separate file)
DEG malignant cells

REFERENCES AND NOTES

1. D. Hanahan, R. A. Weinberg, Hallmarks of cancer: The next generation. *Cell* **144**, 646–674 (2011).

2. N. D. Anderson, R. de Borja, M. D. Young, F. Fuligni, A. Rosic, N. D. Roberts, S. Hajjar, M. Layeghifard, A. Novokmet, P. E. Kowalski, M. Anaka, S. Davidson, M. Zarrei, B. Id Said, L. C. Schreiner, R. Marchand, J. Sitter, N. Gokgoz, L. Brunga, G. T. Graham, A. Fullam, N. Pillay, J. A. Toretsky, A. Yoshida, T. Shibata, M. Metzler, G. R. Somers, S. W. Scherer, A. M. Flanagan, P. J. Campbell, J. D. Schiffman, M. Shago, L. B. Alexandrov, J. S. Wunder, I. L. Andrulis, D. Malkin, S. Behjati, A. Shlien, Rearrangement bursts generate canonical gene fusions in bone and soft tissue tumors. *Science* **361**, eaam8419 (2018).

3. A. G. Henssen, E. Henaff, E. Jiang, A. R. Eisenberg, J. R. Carson, C. M. Villasante, M. Ray, E. Still, M. Burns, J. Gandara, C. Feschotte, C. E. Mason, A. Kentsis, Genomic DNA transposition induced by human PGBD5. *eLife* **4**, e10565 (2015).

4. A. G. Henssen, R. Koche, J. Zhuang, E. Jiang, C. Reed, A. Eisenberg, E. Still, I. C. MacArthur, E. Rodríguez-Fos, S. Gonzalez, M. Puiggròs, A. N. Blackford, C. E. Mason, E. de Stanchina, M. Gönen, A. K. Emde, M. Shah, K. Arora, C. Reeves, N. D. Socci, E. Perlman, C. R. Antonescu, C. W. M. Roberts, H. Steen, E. Mullen, S. P. Jackson, D. Torrents, Z. Weng, S. A. Armstrong, A. Kentsis, PGBD5 promotes site-specific oncogenic mutations in human tumors. *Nat. Genet.* **49**, 1005–1014 (2017).

5. A. G. Henssen, C. Reed, E. Jiang, H. D. Garcia, J. von Stebut, I. C. MacArthur, P. Hundsdoerfer, J. H. Kim, E. de Stanchina, Y. Kuwahara, H. Hosoi, N. J. Ganem, F. dela Cruz, A. L. Kung, J. H. Schulte, J. H. Petrini, A. Kentsis, Therapeutic targeting of PGBD5-induced DNA repair dependency in pediatric solid tumors. *Sci. Transl. Med.* **9**, eaam9078 (2017).

6. L. Helou, L. Beauclair, H. Dardente, P. Arensburger, N. Buisine, Y. Jaszczyszyn, F. Guillou, T. Lecomte, A. Kentsis, Y. Bigot, The C-terminal domain of piggyBac transposase is not required for DNA transposition. *J. Mol. Biol.* **433**, 166805 (2021).

7. L. Helou, L. Beauclair, H. Dardente, B. Piégu, L. Tsakou-Ngouafo, T. Lecomte, A. Kentsis, P. Pontarotti, Y. Bigot, The piggyBac-derived protein 5 (PGBD5) transposes both the closely and the distantly related piggyBac-like elements Tcr-pble and Ifp2. *J. Mol. Biol.* **433**, 166839 (2021).

8. Y. Bigot, M. Yamada, H. Mueller, V. Morell, S. Alves, T. Lecomte, A. Kentsis, Analysis of DNA transposition by DNA transposases in human cells. bioRxiv 2023.04.26.538406 [Preprint] (2023). https://doi.org/10.1101/2023.04.26.538406.

9. G. A. Suero-Abreu, G. Praveen Raju, O. Aristizábal, E. Volkova, A. Wojcinski, E. J. Houston, D. Pham, K. U. Szulc, D. Colon, A. L. Joyner, D. H. Turnbull, In vivo Mn-enhanced MRI for early tumor detection and growth rate analysis in a mouse medulloblastoma model. *Neoplasia* **16**, 993–1006 (2014).

10. P. A. Northcott, I. Buchhalter, A. S. Morrissy, V. Hovestadt, J. Weischenfeldt, T. Ehrenberger, S. Gröbner, M. Segura-Wang, T. Zichner, V. A. Rudneva, H. J. Warnatz, N. Sidiropoulos, A. H. Phillips, S. Schumacher, K. Kleinheinz, S. M. Waszak, S. Erkek, D. T. W. Jones, B. C. Worst, M. Kool, M. Zapatka, N. Jäger, L. Chavez, B. Hutter, M. Bieg, N. Paramasivam, M. Heinold, Z. Gu, N. Ishaque, C. Jäger-Schmidt, C. D. Imbusch, A. Jugold, D. Hübschmann, T. Risch, V. Amstislavskiy, F. G. R. Gonzalez, U. D. Weber, S. Wolf, G. W. Robinson, X. Zhou, G. Wu, D. Finkelstein, Y. Liu, F. M. G. Cavalli, B. Luu, V. Ramaswamy, X. Wu, J. Koster, M. Ryzhova, Y.J. Cho, S. L. Pomeroy, C. Herold-Mende, M. Schuhmann, M. Ebinger, L. M. Liau, J. Mora, R. E. McLendon, N. Jabado, T. Kumabe, E. Chuah, Y. Ma, R. A. Moore, A. J. Mungall, K. L. Mungall, N. Thiessen, K. Tse, T. Wong, S. J. M. Jones, O. Witt, T.

Milde, A. von Deimling, D. Capper, A. Korshunov, M.L. Yaspo, R. Kriwacki, A. Gajjar, J. Zhang, R. Beroukhim, E. Fraenkel, J. O. Korbel, B. Brors, M. Schlesner, R. Eils, M. A. Marra, S. M. Pfister, M. D. Taylor, P. Lichter, The whole-genome landscape of medulloblastoma subtypes. *Nature* **547**, 311–317 (2017).

11. K. M. Reilly, The effects of genetic background of mouse models of cancer: Friend or foe? *Cold Spring Harb. Protoc.* **2016**, pdb top076273 (2016).

12. J. Mao, K. L. Ligon, E. Y. Rakhlin, S. P. Thayer, R. T. Bronson, D. Rowitch, A. P. McMahon, A novel somatic mouse model to survey tumorigenic potential applied to the Hedgehog pathway. *Cancer Res.* **66**, 10171–10178 (2006).

13. Z. Lao, G. P. Raju, C. B. Bai, A. L. Joyner, MASTR: A technique for mosaic mutant analysis with spatial and temporal control of recombination using conditional floxed alleles in mice. *Cell Rep.* **2**, 386–396 (2012).

14. I. L. Tan, A. Wojcinski, H. Rallapalli, Z. Lao, R. M. Sanghrajka, D. Stephen, E. Volkova, A. Korshunov, M. Remke, M. D. Taylor, D. H. Turnbull, A. L. Joyner, Lateral cerebellum is preferentially sensitive to high sonic hedgehog signaling and medulloblastoma formation. *Proc. Natl. Acad. Sci. U.S.A.* **115**, 3392–3397 (2018).

15. P. Gibson, Y. Tong, G. Robinson, M. C. Thompson, D. S. Currle, C. Eden, T. A. Kranenburg, T. Hogg, H. Poppleton, J. Martin, D. Finkelstein, S. Pounds, A. Weiss, Z. Patay, M. Scoggins, R. Ogg, Y. Pei, Z.J. Yang, S. Brun, Y. Lee, F. Zindy, J. C. Lindsey, M. M. Taketo, F. A. Boop, R. A. Sanford, A. Gajjar, S. C. Clifford, M. F. Roussel, P. J. McKinnon, D. H. Gutmann, D. W. Ellison, R. Wechsler-Reya, R. J. Gilbertson, Subtypes of medulloblastoma have distinct developmental origins. *Nature* **468**, 1095–1099 (2010).

16. S. Jessa, A. Blanchet-Cohen, B. Krug, M. Vladoiu, M. Coutelier, D. Faury, B. Poreau, N. de Jay, S. Hébert, J. Monlong, W. T. Farmer, L. K. Donovan, Y. Hu, M. K. McConechy, F. M. G. Cavalli, L. G. Mikael, B. Ellezam, M. Richer, A. Allaire, A. G. Weil, J. Atkinson, J.P. Farmer, R. W. R. Dudley, V. Larouche, L. Crevier, S. Albrecht, M. G. Filbin, H. Sartelet, P.E. Lutz, C. Nagy, G. Turecki, S. Costantino, P. B. Dirks, K. K. Murai, G. Bourque, J. Ragoussis, L. Garzia, M. D. Taylor, N. Jabado, C. L. Kleinman, Stalled developmental programs at the root of pediatric brain tumors. *Nat. Genet.* **51**, 1702–1713 (2019).

17. R. J. Wechsler-Reya, M. P. Scott, Control of neuronal precursor proliferation in the cerebellum by Sonic Hedgehog. *Neuron* **22**, 103–114 (1999).

18. L. V. Goodrich, L. Milenkovic, K. M. Higgins, M. P. Scott, Altered neural cell fates and medulloblastoma in mouse patched mutants. *Science* **277**, 1109–1113 (1997).

19. J. D. Corrales, S. Blaess, E. M. Mahoney, A. L. Joyner, The level of sonic hedgehog signaling regulates the complexity of cerebellar foliation. *Development* **133**, 1811–1821 (2006).

20. A. Flora, T. J. Klisch, G. Schuster, H. Y. Zoghbi, Deletion of *Atoh1* disrupts Sonic Hedgehog signaling in the developing cerebellum and prevents medulloblastoma. *Science* **326**, 1424–1427 (2009).

21. T. G. Oliver, T. A. Read, J. D. Kessler, A. Mehmeti, J. F. Wells, T. T. T. Huynh, S. M. Lin, R. J. Wechsler-Reya, Loss of patched and disruption of granule cell development in a pre-neoplastic stage of medulloblastoma. *Development* **132**, 2425–2439 (2005).

22. E. A. Lumpkin, T. Collisson, P. Parab, A. Omer-Abdalla, H. Haeberle, P. Chen, A. Doetzlhofer, P. White, A. Groves, N. Segil, J. E. Johnson, Math1-driven GFP expression in the developing nervous system of transgenic mice. *Gene Expr. Patterns* **3**, 389–395 (2003).

23. T. Pavelitz, L. T. Gray, S. L. Padilla, A. D. Bailey, A. M. Weiner, PGBD5: A neural-specific intron-containing piggyBac transposase domesticated over 500 million years ago and conserved from cephalochordates to humans. *Mob. DNA* **4**, 23 (2013).

24. A. G. Henssen, E. Jiang, J. Zhuang, L. Pinello, N. D. Socci, R. Koche, M. Gonen, C. M. Villasante, S. A. Armstrong, D. E. Bauer, Z. Weng, A. Kentsis, Forward genetic screen of human transposase genomic rearrangements. *BMC Genomics* **17**, 548 (2016).

25. K. Arora, M. Shah, M. Johnson, R. Sanghvi, J. Shelton, K. Nagulapalli, D. M. Oschwald, M. C. Zody, S. Germer, V. Jobanputra, J. Carter, N. Robine, Deep whole-genome sequencing of 3 cancer cell lines on 2 sequencing platforms. *Sci. Rep.* **9**, 19123 (2019).

26. L. B. Alexandrov, S. Nik-Zainal, D. C. Wedge, S. A. J. R. Aparicio, S. Behjati, A. V. Biankin, G. R. Bignell, N. Bolli, A. Borg, A.-L. Børresen-Dale, S. Boyault, B. Burkhardt, A. P. Butler, C. Caldas, H. R. Davies, C. Desmedt, R. Eils, J. E. Eyfjörd, J. A. Foekens, M. Greaves, F. Hosoda, B. Hutter, T. Ilicic, S. Imbeaud, M. Imielinski, N. Jäger, D. T. W. Jones, D. Jones, S. Knappskog, M. Kool, S. R. Lakhani, C. López-Otín, S. Martin, N. C. Munshi, H. Nakamura, P. A. Northcott, M. Pajic, E. Papaemmanuil, A. Paradiso, J. V. Pearson, X. S. Puente, K. Raine, M. Ramakrishna, A. L. Richardson, J. Richter, P. Rosenstiel, M. Schlesner, T. N. Schumacher, P. N. Span, J. W. Teague, Y. Totoki, A. N. J. Tutt, R. Valdés-Mas, M. M. van Buuren, L. van ‘t Veer, A. Vincent-Salomon, N. Waddell, L. R. Yates; Australian Pancreatic Cancer Genome Initiative; ICGC Breast Cancer Consortium; ICGC MMML-Seq Consortium; ICGC PedBrain, J. Zucman-Rossi, P. A. Futreal, U. M. Dermott, P. Lichter, M. Meyerson, S. M. Grimmond, R. Siebert, E. Campo, T. Shibata, S. M. Pfister, P. J. Campbell, M. R. Stratton, Signatures of mutational processes in human cancer. *Nature* **500**, 415–421 (2013).

27. P. Skowron, H. Farooq, F. M. G. Cavalli, A. S. Morrissy, M. Ly, L. D. Hendrikse, E. Y. Wang, H. Djambazian, H. Zhu, K. L. Mungall, Q. M. Trinh, T. Zheng, S. Dai, A. S. G. Stucklin, M. C. Vladoiu, V. Fong, B. L. Holgado, C. Nor, X. Wu, D. Abd-Rabbo, P. Bérubé, Y. C. Wang, B. Luu, R. A. Suarez, A. Rastan, A. H. Gillmor, J. J. Y. Lee, X. Y. Zhang, C. Daniels, P. Dirks, D. Malkin, E. Bouffet, U. Tabori, J. Loukides, F. P. Doz, F. Bourdeaut, O. O. Delattre, J. Masliah-Planchon, O. Ayrault, S.K. Kim, D. Meyronet, W. A. Grajkowska, C. G. Carlotti, C. de Torres, J. Mora, C. G. Eberhart, E. G. van Meir, T. Kumabe, P. J. French, J. M. Kros, N. Jabado, B. Lach, I. F. Pollack, R. L. Hamilton, A. A. N. Rao, C. Giannini, J. M. Olson, L. Bognár, A. Klekner, K. Zitterbart, J. J. Phillips, R. C. Thompson, M. K. Cooper, J. B. Rubin, L. M. Liau, M. Garami, P. Hauser, K. K. W. Li, H.K. Ng, W. S. Poon, G. Yancey Gillespie, J. A. Chan, S. Jung, R. E. McLendon, E. M. Thompson, D. Zagzag, R. Vibhakar, Y. S. Ra, M. L. Garre, U. Schüller, T. Shofuda, C. C. Faria, E. López-Aguilar, G. Zadeh, C.C. Hui, V. Ramaswamy, S. D. Bailey, S. J. Jones, A. J. Mungall, R. A. Moore, J. A. Calarco, L. D. Stein, G. D. Bader, J. Reimand, J. Ragoussis, W. A. Weiss, M. A. Marra, H. Suzuki, M. D. Taylor, The transcriptional landscape of Shh medulloblastoma. *Nat. Commun.* **12**, 1749 (2021).

28. J. Zhuang, Z. Weng, Local sequence assembly reveals a high-resolution profile of somatic structural variations in 97 cancer genomes. *Nucleic Acids Res.* **43**, 8146–8156 (2015).

29. T. J. Pugh, S. D. Weeraratne, T. C. Archer, D. A. Pomeranz Krummel, D. Auclair, J. Bochicchio, M. O. Carneiro, S. L. Carter, K. Cibulskis, R. L. Erlich, H. Greulich, M. S. Lawrence, N. J. Lennon, A. McKenna, J. Meldrim, A. H. Ramos, M. G. Ross, C. Russ, E. Shefler, A. Sivachenko, B. Sogoloff, P. Stojanov, P. Tamayo, J. P. Mesirov, V. Amani, N. Teider, S. Sengupta, J. P. Francois, P. A. Northcott, M. D. Taylor, F. Yu, G. R. Crabtree, A. G. Kautzman, S. B. Gabriel, G. Getz, N. Jäger, D. T. W. Jones, P. Lichter, S. M. Pfister, T. M.

Roberts, M. Meyerson, S. L. Pomeroy, Y. J. Cho, Medulloblastoma exome sequencing uncovers subtype-specific somatic mutations. *Nature* **488**, 106–110 (2012).

30. M. Kool, D. T. Jones, N. Jäger, P. A. Northcott, T. J. Pugh, V. Hovestadt, R. M. Piro, L. A. Esparza, S. L. Markant, M. Remke, T. Milde, F. Bourdeaut, M. Ryzhova, D. Sturm, E. Pfaff, S. Stark, S. Hutter, H. Seker-Cin, P. Johann, S. Bender, C. Schmidt, T. Rausch, D. Shih, J. Reimand, L. Sieber, A. Wittmann, L. Linke, H. Witt, U. D. Weber, M. Zapatka, R. König, R. Beroukhim, G. Bergthold, P. van Sluis, R. Volckmann, J. Koster, R. Versteeg, S. Schmidt, S. Wolf, C. Lawerenz, C.C. Bartholomae, C. von Kalle, A. Unterberg, C. Herold-Mende, S. Hofer, A. E. Kulozik, A. von Deimling, W. Scheurlen, J. Felsberg, G. Reifenberger, M. Hasselblatt, J. R. Crawford, G. A. Grant, N. Jabado, A. Perry, C. Cowdrey, S. Croul, G. Zadeh, J. O. Korbel, F. Doz, O. Delattre, G. D. Bader, M. McCabe, V. P. Collins, M. W. Kieran, Y. J. Cho, S. L. Pomeroy, O. Witt, B. Brors, M. D. Taylor, U. Schüller, A. Korshunov, R. Eils, R. J. Wechsler-Reya, P. Lichter, S. M. Pfister; ICGC PedBrain Tumor Project, Genome sequencing of SHH medulloblastoma predicts genotype-related response to smoothened inhibition. *Cancer Cell* **25**, 393–405 (2014).

31. M. C. Vladoiu, I. el-Hamamy, L. K. Donovan, H. Farooq, B. L. Holgado, Y. Sundaravadanam, V. Ramaswamy, L. D. Hendrikse, S. Kumar, S. C. Mack, J. J. Y. Lee, V. Fong, K. Juraschka, D. Przelicki, A. Michealraj, P. Skowron, B. Luu, H. Suzuki, A. S. Morrissy, F. M. G. Cavalli, L. Garzia, C. Daniels, X. Wu, M. A. Qazi, S. K. Singh, J. A. Chan, M. A. Marra, D. Malkin, P. Dirks, L. Heisler, T. Pugh, K. Ng, F. Notta, E. M. Thompson, C. L. Kleinman, A. L. Joyner, N. Jabado, L. Stein, M. D. Taylor, Childhood cerebellar tumours mirror conserved fetal transcriptional programs. *Nature* **572**, 67–73 (2019).

32. T. Kato, N. Sato, S. Hayama, T. Yamabuki, T. Ito, M. Miyamoto, S. Kondo, Y. Nakamura, Y. Daigo, Activation of Holliday junction recognizing protein involved in the chromosomal stability and immortality of cancer cells. *Cancer Res.* **67**, 8544–8553 (2007).

33. D. R. Foltz, L. E. T. Jansen, A. O. Bailey, J. R. Yates III, E. A. Bassett, S. Wood, B. E. Black, D. W. Cleveland, Centromere-specific assembly of CENP-a nucleosomes is mediated by HJURP. *Cell* **137**, 472–484 (2009).

34. E. M. Dunleavy, D. Roche, H. Tagami, N. Lacoste, D. Ray-Gallet, Y. Nakamura, Y. Daigo, Y. Nakatani, G. Almouzni-Pettinotti, HJURP is a cell-cycle-dependent maintenance and deposition factor of CENP-A at centromeres. *Cell* **137**, 485–497 (2009).

35. S. Lutolf, F. Radtke, M. Aguet, U. Suter, V. Taylor, Notch1 is required for neuronal and glial differentiation in the cerebellum. *Development* **129**, 373–385 (2002).

36. K. Kitamura, M. Yanazawa, N. Sugiyama, H. Miura, A. Iizuka-Kogo, M. Kusaka, K. Omichi, R. Suzuki, Y. Kato-Fukui, K. Kamiirisa, M. Matsuo, S. I. Kamijo, M. Kasahara, H. Yoshioka, T. Ogata, T. Fukuda, I. Kondo, M. Kato, W. B. Dobyns, M. Yokoyama, K. I. Morohashi, Mutation of ARX causes abnormal development of forebrain and testes in mice and X-linked lissencephaly with abnormal genitalia in humans. *Nat. Genet.* **32**, 359–369 (2002).

37. A. L. Law, S. Jalal, T. Pallett, F. Mosis, A. Guni, S. Brayford, L. Yolland, S. Marcotti, J. A. Levitt, S. P. Poland, M. Rowe-Sampson, A. Jandke, R. Köchl, G. Pula, S. M. Ameer-Beg, B. M. Stramer, M. Krause, Nance-Horan Syndrome-like 1 protein negatively regulates Scar/WAVE-Arp2/3 activity and inhibits lamellipodia stability and cell migration. *Nat. Commun.* **12**, 5687 (2021).

38. A. Kentsis, S. A. Frank, Developmental mutators and early onset cancer. *Front. Pediatr.* **8**, 189 (2020).

39. L. B. Alexandrov, J. Kim, N. J. Haradhvala, M. N. Huang, A. W. T. Ng, Y. Wu, A. Boot, K. R. Covington, D. A. Gordenin, E. N. Bergstrom, S. M. A. Islam, N. Lopez-Bigas, L. J. Klimczak, J. R. McPherson, S. Morganella, R. Sabarinathan, D. A. Wheeler, V. Mustonen; PCAWG Mutational Signatures Working Group, G. Getz, S. G. Rozen, M. R. Stratton; PCAWG Consortium, The repertoire of mutational signatures in human cancer. *Nature* **578**, 94–101 (2020).

40. A. Degasperi, X. Zou, T. D. Amarante, A. Martinez-Martinez, G. C. C. Koh, J. M. L. Dias, L. Heskin, L. Chmelova, G. Rinaldi, V. Y. W. Wang, A. S. Nanda, A. Bernstein, S. E. Momen, J. Young, D. Perez-Gil, Y. Memari, C. Badja, S. Shooter, J. Czarnecki, M. A. Brown, H. R. Davies; Genomics England Research Consortium, S. Nik-Zainal, Substitution mutational signatures in whole-genome–Sequenced cancers in the UK population. *Science* **376**, science.abl.9283 (2022).

41. K. Hadi, X. Yao, J. M. Behr, A. Deshpande, C. Xanthopoulakis, H. Tian, S. Kudman, J. Rosiene, M. Darmofal, J. DeRose, R. Mortensen, E. M. Adney, A. Shaiber, Z. Gajic, M. Sigouros, K. Eng, J. A. Wala, K. O. Wrzeszczyński, K. Arora, M. Shah, A. K. Emde, V. Felice, M. O. Frank, R. B. Darnell, M. Ghandi, F. Huang, S. Dewhurst, J. Maciejowski, T. de Lange, J. Setton, N. Riaz, J. S. Reis-Filho, S. Powell, D. A. Knowles, E. Reznik, B. Mishra, R. Beroukhim, M. C. Zody, N. Robine, K. M. Oman, C. A. Sanchez, M. K. Kuhner, L. P. Smith, P. C. Galipeau, T. G. Paulson, B. J. Reid, X. Li, D. Wilkes, A. Sboner, J. M. Mosquera, O. Elemento, M. Imielinski, Distinct classes of complex structural variation uncovered across thousands of cancer genome graphs. *Cell* **183**, 197–210.e32 (2020).

42. L. Tamayo-Orrego, D. Gallo, F. Racicot, A. Bemmo, S. Mohan, B. Ho, S. Salameh, T. Hoang, A. P. Jackson, G. W. Brown, F. Charron, Sonic hedgehog accelerates DNA replication to

cause replication stress promoting cancer initiation in medulloblastoma *Nat. Cancer* **1**, 840–854 (2021).

43. T. M. Beckermann, W. Luo, C. M. Wilson, R. A. Veach, M. H. Wilson, Cognate restriction of transposition by piggyBac-like proteins. *Nucleic Acids Res.* **49**, 8135–8144 (2021).

44. O. Kolacsek, G. Wachtl, Á. Fóthi, A. Schamberger, S. Sándor, E. Pergel, N. Varga, T. Raskó, Z. Izsvák, Á. Apáti, T. I. Orbán, Functional indications for transposase domestications—Characterization of the human piggyBac transposase derived (PGBD) activities. *Gene* **834**, 146609 (2022).

45. A. Simi, F. Ansaloni, D. Damiani, A. Codino, D. Mangoni, P. Lau, D. Vozzi, L. Pandolfini, R. Sanges, S. Gustincich, The Pgbd5 DNA transposase is required for mouse cerebral cortex development through DNA double-strand breaks formation. bioRxiv 2023.05.09.539730 [Preprint] (2023). https://doi.org/10.1101/2023.05.09.539730.

46. L. J. Zapater, E. Rodriguez-Fos, M. Planas-Felix, S. Lewis, Daniel, Cameron, P. Demarest, A. Nabila, J. Zhao, P. Bergin, C. Reed, Makiko, Yamada, N. D. Socci, M. Hayes, R. Rabadan, D. Torrents, Michael C., Kruer, M. Toth, A. Kentsis, A transposase-derived gene required for human brain development. bioRxiv 2023.04.28.538770 [Preprint] (2023). https://doi.org/10.1101/2023.04.28.538770.

47. R. K. Aziz, M. Breitbart, R. A. Edwards, Transposases are the most abundant, most ubiquitous genes in nature. *Nucleic Acids Res.* **38**, 4207–4217 (2010).

48. R. L. Cosby, J. Judd, R. Zhang, A. Zhong, N. Garry, E. J. Pritham, C. Feschotte, Recurrent evolution of vertebrate transcription factors by transposase capture. *Science* **371**, eabc6405 (2021).

49. M. Hoshino, S. Nakamura, K. Mori, T. Kawauchi, M. Terao, Y. V. Nishimura, A. Fukuda, T. Fuse, N. Matsuo, M. Sone, M. Watanabe, H. Bito, T. Terashima, C. V. E. Wright, Y. Kawaguchi, K. Nakao, Y.I. Nabeshima, Ptf1a, a bHLH transcriptional gene, defines GABAergic neuronal fates in cerebellum. *Neuron* **47**, 201–213 (2005).

50. T. Ellis, I. Smyth, E. Riley, S. Graham, K. Elliot, M. Narang, G. F. Kay, C. Wicking, B. Wainwright, Patched 1 conditional null allele in mice. *Genesis* **36**, 158–161 (2003).

51. R. Machold, G. Fishell, Math1 is expressed in temporally discrete pools of cerebellar rhombic-lip neural progenitors. *Neuron* **48**, 17–24 (2005).

52. J. Jeong, J. Mao, T. Tenzen, A. H. Kottmann, A. P. McMahon, Hedgehog signaling in the neural crest cells regulates the patterning and growth of facial primordia. *Genes Dev.* **18**, 937–951 (2004).

53. A. Wojcinski, A. K. Lawton, N. S. Bayin, Z. Lao, D. N. Stephen, A. L. Joyner, Cerebellar granule cell replenishment postinjury by adaptive reprogramming of Nestin+ progenitors. *Nat. Neurosci.* **20**, 1361–1370 (2017).

54. K. Nakashima, H. Umeshima, M. Kengaku, Cerebellar granule cells are predominantly generated by terminal symmetric divisions of granule cell precursors. *Dev. Dyn.* **244**, 748–758 (2015).

55. H. Y. Lee, L. A. Greene, C. A. Mason, M. C. Manzini, Isolation and culture of post-natal mouse cerebellar granule neuron progenitor cells and neurons. *J. Vis. Exp.* 990 (2009).

56. F. Maura, A. Degasperi, F. Nadeu, D. Leongamornlert, H. Davies, L. Moore, R. Royo, B. Ziccheddu, X. S. Puente, H. Avet-Loiseau, P. J. Campbell, S. Nik-Zainal, E. Campo, N. Munshi, N. Bolli, A practical guide for mutational signature analysis in hematological malignancies. *Nat. Commun.* **10**, 2969 (2019).

57. E. H. Rustad, V. Yellapantula, D. Leongamornlert, N. Bolli, G. Ledergor, F. Nadeu, N. Angelopoulos, K. J. Dawson, T. J. Mitchell, R. J. Osborne, B. Ziccheddu, C. Carniti, V. Montefusco, P. Corradini, K. C. Anderson, P. Moreau, E. Papaemmanuil, L. B. Alexandrov, X. S. Puente, E. Campo, R. Siebert, H. Avet-Loiseau, O. Landgren, N. Munshi, P. J. Campbell, F. Maura, Timing the initiation of multiple myeloma. *Nat. Commun.* **11**, 1917 (2020).

58. Z. Sondka, S. Bamford, C. G. Cole, S. A. Ward, I. Dunham, S. A. Forbes, The COSMIC Cancer Gene Census: Describing genetic dysfunction across all human cancers. *Nat. Rev. Cancer* **18**, 696–705 (2018).

59. T. L. Bailey, C. Elkan, Fitting a mixture model by expectation maximization to discover motifs in biopolymers. *Proc. Int. Conf. Intell. Syst. Mol. Biol.* **2**, 28–36 (1994).

60. T. L. Bailey, M. Boden, F. A. Buske, M. Frith, C. E. Grant, L. Clementi, J. Ren, W. W. Li, W. S. Noble, MEME SUITE: Tools for motif discovery and searching. *Nucleic Acids Res.* **37**, W202–W208 (2009).

61. S. Gupta, J. A. Stamatoyannopoulos, T. L. Bailey, W. S. Noble, Quantifying similarity between motifs. *Genome Biol.* **8**, R24 (2007).

62. I. Masilionis, O. Chaudhary, B. M. Urben, R. Chaligne, Nuclei extraction for 10x Genomics Single Cell Multiome ATAC + Gene Expression from frozen tissue using Singulator™ 100 or 200 (S2 Genomics) V2.0. protocols.io (2023).

63. T. Stuart, A. Srivastava, S. Madad, C. A. Lareau, R. Satija, Single-cell chromatin state analysis with Signac. *Nat. Methods* **18**, 1333–1341 (2021).

64. Y. Hao, S. Hao, E. Andersen-Nissen, W. M. Mauck III, S. Zheng, A. Butler, M. J. Lee, A. J. Wilk, C. Darby, M. Zager, P. Hoffman, M. Stoeckius, E. Papalexi, E. P. Mimitou, J. Jain, A. Srivastava, T. Stuart, L. M. Fleming, B. Yeung, A. J. Rogers, J. M. McElrath, C. A. Blish, R.

Gottardo, P. Smibert, R. Satija, Integrated analysis of multimodal single-cell data. *Cell* **184**, 3573–3587.e29 (2021).

65. Y. Zhang, T. Liu, C. A. Meyer, J. Eeckhoute, D. S. Johnson, B. E. Bernstein, C. Nusbaum, R. M. Myers, M. Brown, W. Li, X. S. Liu, Model-based analysis of ChIP-Seq (MACS). *Genome Biol.* **9**, R137 (2008).

66. T. Stuart, A. Butler, P. Hoffman, C. Hafemeister, E. Papalexi, W. M. Mauck III, Y. Hao, M. Stoeckius, P. Smibert, R. Satija, Comprehensive Integration of Single-Cell Data. *Cell* **177**, 1888–1902.e21 (2019).

67. L. McInnes, J. Healy, J. Melville, UMAP: Uniform Manifold Approximation and Projection for dimension reduction. arXiv:1802.03426 [stat.ML] (2018).

68. I. Korsunsky, N. Millard, J. Fan, K. Slowikowski, F. Zhang, K. Wei, Y. Baglaenko, M. Brenner, P. R. Loh, S. Raychaudhuri, Fast, sensitive and accurate integration of single-cell data with Harmony. *Nat. Methods* **16**, 1289–1296 (2019).

69. C. Li, *B. Liu, B. Kang, Z. Liu, Y. Liu, C. Chen, X. Ren, Z. Zhang*, SciBet as a portable and fast single cell type identifier. *Nat. Commun.* **11**, 1818 (2020).

70. Y. Tan, P. Cahan, SingleCellNet: A computational tool to classify single cell RNA-seq data across platforms and across species. *Cell Syst.* **9**, 207–213.e2 (2019).

71. D. Aran, A. P. Looney, L. Liu, E. Wu, V. Fong, A. Hsu, S. Chak, R. P. Naikawadi, P. J. Wolters, A. R. Abate, A. J. Butte, M. Bhattacharya, Reference-based analysis of lung single-cell sequencing reveals a transitional profibrotic macrophage. *Nat. Immunol.* **20**, 163–172 (2019).

72. S. Jessa, A. Mohammadnia, A. S. Harutyunyan, M. Hulswit, S. Varadharajan, H. Lakkis, N. Kabir, Z. Bashardanesh, S. Hébert, D. Faury, M. C. Vladoiu, S. Worme, M. Coutelier, B. Krug, A. Faria Andrade, M. Pathania, A. Bajic, A. G. Weil, B. Ellezam, J. Atkinson, R. W. R. Dudley,

J.P. Farmer, S. Perreault, B. A. Garcia, V. Larouche, M. Blanchette, L. Garzia, A. Bhaduri, K. L. Ligon, P. Bandopadhayay, M. D. Taylor, S. C. Mack, N. Jabado, C. L. Kleinman, K27M in canonical and noncanonical H3 variants occurs in distinct oligodendroglial cell lineages in brain midline gliomas. *Nat. Genet.* **54**, 1865–1880 (2022).

73. T. Tickle, I. Tirosh, C. Georgescu, M. Brown, B. Haas, inferCNV of the Trinity CTAT Project. Klarman Cell Observatory, Broad Institute of MIT and Harvard, Cambridge, MA, USA (2019).

74. A. M. Bolger, M. Lohse, B. Usadel, Trimmomatic: A flexible trimmer for Illumina sequence data. *Bioinformatics* **30**, 2114–2120 (2014).

75. A. Dobin, C. A. Davis, F. Schlesinger, J. Drenkow, C. Zaleski, S. Jha, P. Batut, M. Chaisson, T. R. Gingeras, STAR: Ultrafast universal RNA-seq aligner. *Bioinformatics* **29**, 15–21 (2013).

76. Y. Liao, G. K. Smyth, W. Shi, featureCounts: An efficient general purpose program for assigning sequence reads to genomic features. *Bioinformatics* **30**, 923–930 (2014).

77. M. I. Love, W. Huber, S. Anders, Moderated estimation of fold change and dispersion for RNA-seq data with DESeq2. *Genome Biol.* **15**, 550 (2014).

78. P. A. Northcott, D. J. H. Shih, J. Peacock, L. Garzia, A. Sorana Morrissy, T. Zichner, A. M. Stütz, A. Korshunov, J. Reimand, S. E. Schumacher, R. Beroukhim, D. W. Ellison, C. R. Marshall, A. C. Lionel, S. Mack, A. Dubuc, Y. Yao, V. Ramaswamy, B. Luu, A. Rolider, F. M. G. Cavalli, X. Wang, M. Remke, X. Wu, R. Y. B. Chiu, A. Chu, E. Chuah, R. D. Corbett, G. R. Hoad, S. D. Jackman, Y. Li, A. Lo, K. L. Mungall, K. Ming Nip, J. Q. Qian, A. G. J. Raymond, N. Thiessen, R. J. Varhol, I. Birol, R. A. Moore, A. J. Mungall, R. Holt, D. Kawauchi, M. F. Roussel, M. Kool, D. T. W. Jones, H. Witt, A. Fernandez-L, A. M. Kenney, R. J. Wechsler-Reya, P. Dirks, T. Aviv, W. A. Grajkowska, M. Perek-Polnik, C. C. Haberler, O. Delattre, S. S.

Reynaud, F. F. Doz, S. S. Pernet-Fattet, B.K. Cho, S.K. Kim, K.C. Wang, W. Scheurlen, C. G. Eberhart, M. Fèvre-Montange, A. Jouvet, I. F. Pollack, X. Fan, K. M. Muraszko, G. Yancey Gillespie, C. di Rocco, L. Massimi, E. M. C. Michiels, N. K. Kloosterhof, P. J. French, J. M. Kros, J. M. Olson, R. G. Ellenbogen, K. Zitterbart, L. Kren, R. C. Thompson, M. K. Cooper, B. Lach, R. E. McLendon, D. D. Bigner, A. Fontebasso, S. Albrecht, N. Jabado, J. C. Lindsey, S. Bailey, N. Gupta, W. A. Weiss, L. Bognár, A. Klekner, T. E. van Meter, T. Kumabe, T. Tominaga, S. K. Elbabaa, J. R. Leonard, J. B. Rubin, L. M. Liau, E. G. van Meir, M. Fouladi, H. Nakamura, G. Cinalli, M. Garami, P. Hauser, A. G. Saad, A. Iolascon, S. Jung, C. G. Carlotti, R. Vibhakar, Y. Shin Ra, S. Robinson, M. Zollo, C. C. Faria, J. A. Chan, M. L. Levy, P. H. B. Sorensen, M. Meyerson, S. L. Pomeroy, Y.J. Cho, G. D. Bader, U. Tabori, C. E. Hawkins, E. Bouffet, S. W. Scherer, J. T. Rutka, D. Malkin, S. C. Clifford, S. J. M. Jones, J. O. Korbel, S. M. Pfister, M. A. Marra, M. D. Taylor, Subgroup-specific structural variation across 1,000 medulloblastoma genomes. *Nature* **488**, 49–56 (2012).

79. R. J. Gilbertson, S. C. Clifford, W. MacMeekin, W. Meekin, C. Wright, R. H. Perry, P. Kelly, A.D. Pearson, J. Lunec, Expression of the ErbB-neuregulin signaling network during human cerebellar development: Implications for the biology of medulloblastoma. *Cancer Res.* **58**, 3932–3941 (1998).

80. J. Aldaregia, P. Errarte, A. Olazagoitia-Garmendia, M. Gimeno, J. J. Uriz, T. R. Gershon, I. Garcia, A. Matheu, Erbb4 is required for cerebellar developmentand malignant phenotype of medulloblastoma. *Cancers* **12**, 997 (2020).

81. C. Gu, N. Yokota, Y. Gao, J. Yamamoto, T. Tokuyama, H. Namba, Gene expression of growth signaling pathways is up-regulated in CD133-positive medulloblastoma cells. *Oncol. Lett.* **2**, 357–361 (2011).

82. H. Fukushima, R. Suzuki, Y. Yamaki, S. Hosaka, M. Inaba, A. Muroi, T. Tsurubuchi, W. Morii, E. Noguchi, H. Takada, Cancer-predisposition genetic analysis in children with brain tumors treated at a single institution in Japan. *Oncology* **100**, 163–172 (2022).

83. W. P. Kloosterman, J. Koster, J. J. Molenaar, Prevalence and clinical implications of chromothripsis in cancer genomes. *Curr. Opin. Oncol.* **26**, 64–72 (2014).

84. A. Thomaz, M. Jaeger, A. L. Brunetto, A. T. Brunetto, L. Gregianin, C. B. de Farias, V. Ramaswamy, C. Nör, M. D. Taylor, R. Roesler, Neurotrophin signaling in medulloblastoma. *Cancers* **12**, 2542 (2020).

85. P. A. Northcott, D. T. W. Jones, M. Kool, G. W. Robinson, R. J. Gilbertson, Y. J. Cho, S. L. Pomeroy, A. Korshunov, P. Lichter, M. D. Taylor, S. M. Pfister, Medulloblastomics: The end of the beginning. *Nat. Rev. Cancer* **12**, 818–834 (2012).

86. P. A. Northcott, C. Lee, T. Zichner, A. M. Stütz, S. Erkek, D. Kawauchi, D. J. H. Shih, V. Hovestadt, M. Zapatka, D. Sturm, D. T. W. Jones, M. Kool, M. Remke, F. M. G. Cavalli, S. Zuyderduyn, G. D. Bader, S. VandenBerg, L. A. Esparza, M. Ryzhova, W. Wang, A. Wittmann, S. Stark, L. Sieber, H. Seker-Cin, L. Linke, F. Kratochwil, N. Jäger, I. Buchhalter, C. D. Imbusch, G. Zipprich, B. Raeder, S. Schmidt, N. Diessl, S. Wolf, S. Wiemann, B. Brors, C. Lawerenz, J. Eils, H.J. Warnatz, T. Risch, M.L. Yaspo, U. D. Weber, C. C. Bartholomae, C. von Kalle, E. Turányi, P. Hauser, E. Sanden, A. Darabi, P. Siesjö, J. Sterba, K. Zitterbart, D. Sumerauer, P. van Sluis, R. Versteeg, R. Volckmann, J. Koster, M. U. Schuhmann, M. Ebinger, H. L. Grimes, G. W. Robinson, A. Gajjar, M. Mynarek, K. von Hoff, S. Rutkowski, T. Pietsch, W. Scheurlen, J. Felsberg, G. Reifenberger, A. E. Kulozik, A. von Deimling, O. Witt, R. Eils, R. J. Gilbertson, A. Korshunov, M. D. Taylor, P. Lichter, J. O. Korbel, R. J. Wechsler-Reya, S. M. Pfister, Enhancer hijacking activates GFI1 family oncogenes in medulloblastoma. *Nature* **511**, 428–434 (2014).